



**HAL**  
open science

# A Variable Chirp Rate Stepped Frequency Linear Frequency Modulation Waveform Designed to Approximate Wideband Non-Linear Radar Waveforms

Mahdi Saleh, Samir-Mohamad Omar, Eric Grivel, Pierrick Legrand

► **To cite this version:**

Mahdi Saleh, Samir-Mohamad Omar, Eric Grivel, Pierrick Legrand. A Variable Chirp Rate Stepped Frequency Linear Frequency Modulation Waveform Designed to Approximate Wideband Non-Linear Radar Waveforms. Digital Signal Processing, 2020, 10.1016/j.dsp.2020.102884 . hal-02963775

**HAL Id: hal-02963775**

**<https://hal.science/hal-02963775>**

Submitted on 15 Dec 2022

**HAL** is a multi-disciplinary open access archive for the deposit and dissemination of scientific research documents, whether they are published or not. The documents may come from teaching and research institutions in France or abroad, or from public or private research centers.

L'archive ouverte pluridisciplinaire **HAL**, est destinée au dépôt et à la diffusion de documents scientifiques de niveau recherche, publiés ou non, émanant des établissements d'enseignement et de recherche français ou étrangers, des laboratoires publics ou privés.



Distributed under a Creative Commons Attribution - NonCommercial 4.0 International License

# A Variable Chirp Rate Stepped Frequency Linear Frequency Modulation Waveform Designed to Approximate Wideband Non-Linear Radar Waveforms

Mahdi Saleh<sup>a,b,\*</sup>, Samir-Mohamad Omar<sup>b,c</sup>, Eric Grivel<sup>a</sup>, Pierrick Legrand<sup>d</sup>

<sup>a</sup>Bordeaux University - Bordeaux INP ENSEIRB-MATMECA - IMS - UMR CNRS 5218, Talence, FRANCE

<sup>b</sup>Department of Physics and Electronics, Faculty of Sciences I, Lebanese University, Hadath, Beirut, LEBANON

<sup>c</sup>CCE Department, School of Engineering, International University of Beirut (BIU), Beirut, Lebanon

<sup>d</sup>Bordeaux University - IMB UMR CNRS 5251 - INRIA, FRANCE

---

## Abstract

The non-linear frequency modulation (NLFM) waveform is one of the existing waveforms that can be used in high range resolution radar applications. However, a high sampling frequency and consequently an expensive ADC are required. To overcome this drawback while taking advantage of the features of the NLFM waveform, we suggest approximating the wideband NLFM waveform by a piecewise linear waveform and using it in a stepped frequency (SF) framework. Thus, a variable chirp rate SF-LFM waveform is proposed where SF is combined with a train of LFM pulses having different chirp rates, durations, and bandwidths. In this paper, these parameters are derived from a tangent-based NLFM waveform. At the receiver, a generalized version of the time domain (TD) algorithm is proposed to process the received echoes. Our purpose is to obtain the high range resolution profile (HRRP) whose properties are of the same magnitude orders as those obtained using a tangent-based NLFM waveform. These properties are the peak sidelobe ratio, the integrated sidelobe, and the range resolution. Toward this goal, a multi-objective optimization issue is addressed to deduce the parameters of the proposed waveform by using two types of approaches based on evolutionary algorithms. Their relevance is compared. Our analysis and simulations show that the proposed approaches attain the targeted performance goals with a smaller sampling frequency at the receiver.

**Keywords:** Stepped frequency waveforms, piecewise NLFM, peak sidelobe ratio, time domain algorithm, multi-objective optimization, genetic algorithm, NSGA-II.

---

## 1. Introduction

Over the last decades, the demand for attaining high range resolution (HRR) in radar has steadily increased. It is considered as one of the most essential metrics in various radar applications from ground penetrating radar (GPR) and synthetic aperture radar (SAR) to target recognition radar.

The range resolution of the radar can be enhanced by using two main families of approaches:

On the one hand, a waveform that exploits one of the pulse compression techniques can be considered. However, as it possesses a high instantaneous bandwidth, an expensive analog-to-digital converter (ADC) is required. Among the pulse compression techniques, the linear frequency modulation (LFM) is the most popular one. This is probably due to its simplicity to be generated and its Doppler tolerance [1]. At the receiver, a matched filter (MF) is applied to the received LFM pulses to maximize the signal-to-noise

ratio (SNR) at the MF output. In this case, the MF output represents the high range resolution profile<sup>1</sup> (HRRP). For a single-point stationary target and without additive disturbances, the mainlobe width and the sidelobe levels of the MF output are characterized by the correlation function of the LFM waveform. To reduce the sidelobe levels, an amplitude windowing is generally combined with a MF done in the frequency domain. This comes at the cost of a smaller SNR at the output of the MF and an increase of the mainlobe width. As an alternative, a non-linear frequency modulation (NLFM) can be used. There are some waveforms that are "naturally" NLFM, such as the hybrid NLFM [2], the tangent-based, and the sine-based waveforms [3] [4]. However, others can be designed to meet certain requirements. Thus, the principle of stationary phase can be used to synthesize an NLFM waveform that has a power spectral density (PSD) similar to certain well-known windows such as the Taylor and Blackman-Harris windows [5] [6]. In [7], the authors exploited the principle of stationary phase to derive a mathematical model in which the non-linear time-frequency relation is expressed

---

\*Corresponding author

Email addresses: [mahdi.saleh@u-bordeaux.fr](mailto:mahdi.saleh@u-bordeaux.fr) (Mahdi Saleh),  
[samir.omar@liu.edu.lb](mailto:samir.omar@liu.edu.lb) (Samir-Mohamad Omar),  
[eric.grivel@ims-bordeaux.fr](mailto:eric.grivel@ims-bordeaux.fr) (Eric Grivel),  
[pierrick.legrand@u-bordeaux.fr](mailto:pierrick.legrand@u-bordeaux.fr) (Pierrick Legrand)

<sup>1</sup>HRRP is representative of the reflectivity of the target to an HRR radar waveform projected onto the radar line-of-sight.

as the combination of a linear function and a sine series. In [8] a high-precision NLFM signal generator with the ability of predistortion compensation is developed. A train of piecewise linear functions [9] can also be considered. For instance, the authors in [10] proposed what they called a single-carrier piecewise NLFM (SC-PW-NLFM) waveform. It consists of two symmetric sets, where each one is composed of  $N + 1$  consecutive linear chirp subpulses with different bandwidths and pulse widths. The corresponding instantaneous frequency  $f(t)$  occupies a global band equal to  $B$  Hz during the time  $T_p$  and has two main properties: Firstly, it is a piecewise continuous linear function of the time. Secondly,  $f(t) = B - f(T_p - t)$  for  $0 \leq t \leq \frac{T_p}{2}$ . It should be noted that with NLFM waveforms, there is no need to apply an amplitude windowing to the MF output since the sidelobe levels are low. Hence, the SNR at the MF output is maximized with no losses. However, the NLFM waveform is less Doppler tolerant than the LFM one [3].

On the other hand, a waveform with a large bandwidth distributed among the pulses can be considered. This waveform exhibits a small instantaneous bandwidth. The most attractive one is the stepped frequency (SF) waveform [11] [12] [5]. It is composed of narrow-band pulses with different equally-spaced carrier frequencies. The corresponding received pulses are coherently combined at the receiver to obtain the HRRP. Using SF waveforms makes it possible to exploit an ADC with a small sampling rate. Moreover, it reduces the dispersion effects in some systems such as phased array radar [5]. At the receiver, the HRRP of a target induced by the SF waveforms can be obtained with two different approaches. In the first one, the MF is applied to the whole train of the received echoes. It requires a high computational power. In the second one, three algorithms exist, namely the Inverse Fast Fourier Transform (IFFT), the frequency domain (FD) algorithm, and the time domain (TD) algorithm [11]. The FD and IFFT algorithms have a relatively-low computational cost. As for the TD algorithm, it has been only investigated with a SF-LFM waveform where a train of LFM pulses having the same chirp rates, durations, and bandwidths is processed at the receiver [13].

The above two families can be used separately or together. In various radar applications, the SF waveform can be combined with one of the pulse compression techniques to reduce the number of transmitted pulses within the coherent processing interval (CPI) [14]. Thus, the SF-LFM waveform [15] [16] [17] [18], the SF phase coding (SFPC) [19] [20], and the SF-NLFM [21] are studied in the literature. Furthermore, in [22] and [23], special efforts were made to reduce both the grating lobes and the peak sidelobes of the autocorrelation function of the SF-LFM waveform. In [24], a framework for ISAR imaging is proposed through sparse stepped-frequency waveforms (SSFWs) where some portions of frequency subbands are used to reconstruct full-resolution images by exploiting sparsity.

Recently, in [25], a new way has been proposed to com-

bine SF with PC or NLFM. This has the advantage of overcoming the drawbacks of the standard combination. It consists in splitting the spectrum of a PC or NLFM pulse into a predetermined number of portions and then transmitting the corresponding time-domain signals. At the receiver, a modified FD algorithm has been proposed to produce the HRRP. The latter algorithm does not necessarily provide significant results when  $N_p$  becomes large, the reconstruction of the power spectrum of the waveform being strongly distorted. To overcome this drawback, a TWR algorithm has been proposed in [26].

In order to fairly compare the properties of the waveforms in a radar system, some criteria must be taken into account, such as the computational cost and the sampling frequency at the receiver. In addition, designers usually aim at maximizing the probability of detection (PD) for a given probability of false alarm. For this purpose, various performance measures are taken into consideration due to their great influences on the PD. Among them, two characterize the HRRP. These are the peak sidelobe ratio (PSLR) and the integrated sidelobe ratio (ISLR) [27] [28]. In this paper, in order to avoid the hardware complexities that may occur when transmitting a wideband SC-PW-NLFM within a single pulse, we propose a SF-LFM waveform with a variable chirp rate. It consists of a train of narrow-band LFM pulses with different chirp rates that are derived from an NLFM waveform. In this paper, a tangent-based NLFM is considered to illustrate our point. However, our proposed scheme is applicable to any NLFM waveform. To produce the HRRP at the receiver, we propose a generalized version of the TD algorithm to process the back-scattered echoes. This processing chain in the presence of narrow-band LFM pulses at the receiver makes it possible to use an ADC with a sampling rate smaller than that used for the wideband NLFM waveform. In counterpart, an interpolation step has then to be added to be able to retrieve the wideband NLFM waveform in the time domain. Our goal is to obtain an HRRP that could be as similar as possible as that of the tangent-based NLFM waveform while using a much smaller sampling frequency. To this end, the parameters of this train are selected by addressing a multi-objective issue. The latter is defined from three different criteria related to the PSLR, the ISLR, and the range resolution of the waveform. They aim at getting PSLR, ISLR and range resolution as close as possible to those obtained with the tangent-based NLFM waveform. However, minimizing one of these criteria does not necessarily reduce the two others. As no analytic expression of the parameters can be obtained easily, we suggest using two types of approaches. The first one is a genetic algorithm where the fitness function to be minimized is a weighted sum of the three criteria to be taken into account. In this case, one solution is obtained for a set of weights. The second one is derived from the NSGA-II, which is a fast sorting and elite multi-objective genetic algorithm that was initially proposed in [29]. It provides Pareto fronts. It should be noted that both are designed

to take into account a constraint on the selection of the durations of the LFM pulses.

The remainder of this paper is organized as follows: first of all, the processing chain of the SC tangent based NLFM waveform is presented in section 2. It makes it possible to introduce some concepts such as the HRRP, the PSLR, the ISLR and the range resolution. In section 3, the SF-LFM waveform is recalled, and its generalization with a variable chirp rate is introduced. The processing chain of this waveform is presented. This includes what is done at the transmitter and the receiver. In section 4, the optimization issue is addressed. A brief presentation of the two approaches we suggest using is done. In section 5, simulation results, as well as comments, are provided. In section 6, the relevance of our approach is analyzed to check its reliability in the presence of multiple targets and Doppler effect. Conclusions and perspectives end the paper.

## 2. Preamble: processing chain of the SC tangent-based NLFM waveform

In this section, the standard processing chain of the SC tangent-based NLFM waveform is presented. The description of this waveform will be useful in the rest of the paper. Moreover, some performance measures related to the HRRP are defined.

### 2.1. At the transmitter: definition of the waveform

The SC tangent-based NLFM transmitted waveform can be formulated as follows:

$$s_{tx}(t) = A \text{rect}\left(\frac{t - \frac{T_p}{2}}{T_p}\right) \exp\left(j\phi\left(t - \frac{T_p}{2}\right)\right) \exp(j2\pi f_c t) \quad (1)$$

where  $A$  is the magnitude,  $\text{rect}(t)$  stands for a rectangular pulse equal to 1 for  $-\frac{1}{2} \leq t \leq \frac{1}{2}$  and zero elsewhere,  $T_p$  is the pulse duration,  $f_c$  is the carrier frequency and  $\phi(t)$  is the instantaneous phase. The latter is related to the instantaneous frequency for  $-\frac{T_p}{2} \leq t \leq \frac{T_p}{2}$  as follows [3]:

$$f(t) = \frac{1}{2\pi} \frac{d\phi(t)}{dt} = B \frac{\tan(2\beta t/T_p)}{2 \tan \beta} = -f(-t) \quad (2)$$

where  $B$  is the total bandwidth covered by the waveform during  $T_p$  since  $f(t)$  varies between  $-\frac{B}{2}$  and  $\frac{B}{2}$  where:

$$\begin{cases} f(-\frac{T_p}{2}) = -\frac{B}{2} \\ f(\frac{T_p}{2}) = \frac{B}{2} \end{cases} \quad (3)$$

In addition,  $\beta \in [0, \pi/2]$  is a parameter that can be adjusted by the practitioner. When  $\beta$  tends to 0, this corresponds to the linear frequency modulation (LFM) case. The degree of non-linearity increases with  $\beta$ , as shown in Fig. 1.

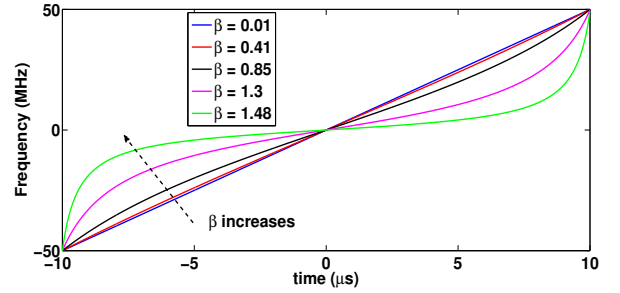


Figure 1: Instantaneous frequency of the SC tangent-based NLFM waveform for different values of  $\beta$  with  $B = 100$  MHz and  $T_p = 20$   $\mu\text{s}$ .

### 2.2. At the receiver: demodulation, matched filtering, HRRP, and features characterizing it

The received signal is a delayed version of the transmitted waveform disturbed by additive disturbances. It can be modeled by:

$$s_{rx}(t) = \alpha s_{tx}(t - t_d) + \eta(t) \quad (4)$$

where  $t_d = \frac{2R}{c}$  is the time delay that corresponds to the range  $R$  of the target and  $c$  is the speed of light. In addition,  $\eta(t)$  corresponds to the disturbances such as the measurement white noise and the clutter, and  $\alpha$  is an attenuation coefficient that depends on many factors including among others the radar cross section (RCS) of the target, the range, and the frequency of the waveform. In the sequel, for the sake of space, especially in the equations, we focus our attention on the signal part. Nevertheless, each step of the algorithm is also applied to the disturbances. Thus, the "ideal"<sup>2</sup> received signal can be modeled by:

$$s_{rx}(t) = A \text{rect}\left(\frac{t - \frac{T_p}{2} - t_d}{T_p}\right) \exp\left(j\phi\left(t - \frac{T_p}{2} - t_d\right)\right) \times \exp(j2\pi f_c(t - t_d)) \quad (5)$$

The latter is first demodulated as shown below:

$$s_d(t) = s_{rx}(t) \exp(-j2\pi f_c t) = \exp\left(-j2\pi f_c t_d\right) \times A \text{rect}\left(\frac{t - \frac{T_p}{2} - t_d}{T_p}\right) \exp\left(j\phi\left(t - \frac{T_p}{2} - t_d\right)\right) \quad (6)$$

Then, the demodulated signal is sampled at a sampling rate  $F_s = \frac{1}{T_s} = B$  Hz. Hence, given the expression of  $t_d$ , the  $n^{\text{th}}$  sample of the demodulated received signal is equal to:

$$s_d(n) = A \exp\left(j\phi\left(nT_s - \frac{T_p}{2} - \frac{2R}{c}\right)\right) \exp\left(-j2\pi f_c \frac{2R}{c}\right) \quad (7)$$

In (7),  $n \in \llbracket 0, L-1 \rrbracket$  where  $L$  denotes the number of samples associated with the received pulse. It is equal to  $\frac{T_p}{T_s}$  in the ideal case. Otherwise,  $L = \lfloor \frac{T_p}{T_s} \rfloor$ , where  $\lfloor \cdot \rfloor$  is the floor function.

<sup>2</sup>i.e. without disturbance and attenuation coefficient.

At this level, the HRRP can be created by applying a MF to (7). It consists in convolving  $s_d(n)$  with the conjugate of the reference signal,  $s_{ref}(-n) = \exp\left(j\phi\left(-nT_s - \frac{T_p}{2}\right)\right)$ . The latter can hence be deduced from the ambiguity function.

The HRRP usually exhibits a mainlobe and sidelobes. The levels of the sidelobes have a great influence on the performance of detection [30]. Therefore, three different measures are usually considered to characterize the HRRP.

In the following, the **peak sidelobe ratio (PSLR)** and the **integrated sidelobe ratio (ISLR)** are respectively given by:

$$\begin{cases} PSLR = 20\log\left[\frac{\max(\text{sidelobe peak})}{\text{mainlobe peak}}\right] \\ ISLR = 10\log\left[\frac{\text{total energy in sidelobes}}{\text{energy in mainlobe}}\right] \end{cases} \quad (8)$$

Finally, various criteria are used to define the range resolution. Two of the more common criteria used to define it are [1]:

- The 3-dB width of the mainlobe which defines the range resolution as the separation between the peak point and the point that corresponds to the half of the peak power.
- The Rayleigh criterion which defines the range resolution as the separation between the peak and the null.

In this paper, the first criterion is used.

When the SC tangent-based NLFM waveform is used in high range resolution radar applications, a high sampling frequency is required. Consequently, expensive ADCs must be used. To overcome this drawback, a SF waveform would be of interest. In the next section, we propose a SF inspired scheme.

### 3. Our proposed waveform from the transmitter to the receiver

In this section, we present two of our contributions: firstly, the generalization of the standard SF-LFM waveform whose chirp rate varies from pulse to pulse is presented. The latter is called 'variable chirp rate SF-LFM', whose parameters correspond to a set of pulse bandwidths and durations. We show how to derive them from an NLFM waveform. In this paper and without loss of generality, we suggest considering the SC tangent-based NLFM presented in the preamble. Secondly, the whole processing chain from the transmitter to the receiver is detailed. More particularly, we present how the parameters of the waveform are exploited to construct a train of baseband pulses at the transmitter and how the received signals are processed to produce the HRRP. We will see that one of the key issues is to guarantee the continuity of the phase, especially when one aims at reducing the sampling frequency at the receiver.

#### 3.1. From the SF-LFM waveform to the variable chirp rate SF-LFM waveform

##### 3.1.1. About the SF-LFM waveform

The SF-LFM radar transmits a burst of  $N_p$  linear modulated pulses, whose carrier frequency monotonically varies from pulse to pulse by a fixed frequency step size denoted as  $\Delta f$ , as shown in Fig. 2. For the  $(m+1)^{th}$  pulse ( $m \in \llbracket 0, N_p - 1 \rrbracket$ ) which corresponds to the time interval  $mT_r \leq t \leq mT_r + T_p$ , the transmitted waveform is defined as follows:

$$s_{tx,m}(t) = v_m(t)\exp(j2\pi f_c^{(m)}t) \quad (9)$$

where:

- $v_m(t)$  is the  $(m+1)^{th}$  baseband LFM pulse defined by:

$$\begin{aligned} v_m(t) = & \text{Arect}\left(\frac{t - mT_r - \frac{T_p}{2}}{T_p}\right) \\ & \times \exp\left(j\pi\gamma\left(t - mT_r - \frac{T_p}{2}\right)^2\right) \end{aligned} \quad (10)$$

In (10),  $A$  is the magnitude.  $T_p$  and  $T_r$  denote the pulse width and the pulse repetition interval respectively. If  $B_p$  is the passband bandwidth of each pulse, the chirp rate  $\gamma$  is given by:

$$\gamma = \frac{B_p}{T_p} \quad (11)$$

In addition, the instantaneous frequency of each pulse is:

$$f(t) = \gamma\left(t - mT_r - \frac{T_p}{2}\right) \quad (12)$$

When  $t = mT_r$ ,  $f(t) = -B_p/2$  whereas  $f(t) = B_p/2$  for  $t = mT_r + T_p$ .

- The carrier frequency of the  $(m+1)^{th}$  transmitted pulse is given by:

$$f_c^{(m)} = f_c + \Delta f^{(m)} \quad (13)$$

where

$$\Delta f^{(m)} = \left(\frac{1 - N_p}{2} + m\right)\Delta f \quad (14)$$

with  $f_c$  the central carrier frequency of the complete train of pulses. Usually,  $\Delta f$  is smaller than  $B_p$  to avoid creating gaps in the transmitted waveform. When  $\Delta f = B_p$ , the total bandwidth covered by the waveform is  $B = N_p B_p$ .

It is true that with the standard SF waveforms, the carrier frequency monotonically changes either in an increasing or decreasing order. However, an alternative exists where the carrier frequency can change from pulse to pulse using the Costas codes [31].

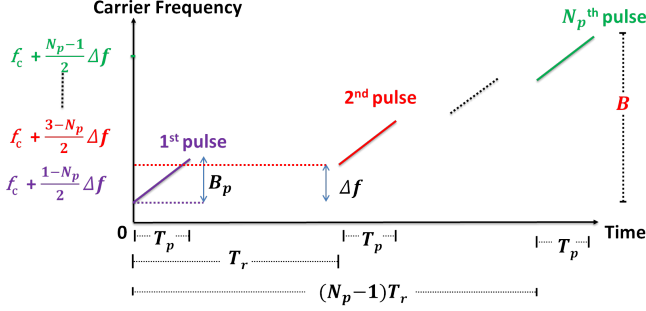


Figure 2: The standard Stepped frequency linear frequency modulated waveform.

### 3.1.2. Generalization of the SF-LFM waveform: the variable chirp rate SF-LFM waveform

In this paper, we suggest generalizing the above waveform by modifying the bandwidth and the pulse duration from one pulse to another. In this case, the chirp rate varies from one pulse to another, as shown in Fig. 3. Its notation becomes for the  $(m+1)^{th}$  pulse, with  $m = 0, \dots, N_p - 1$ :

$$\gamma^{(m)} = \frac{B_p^{(m)}}{T_p^{(m)}} \quad (15)$$

where  $B_p^{(m)}$  and  $T_p^{(m)}$  respectively denote the passband bandwidth and the duration of the  $(m+1)^{th}$  pulse, with  $\sum_{m=0}^{N_p-1} B_p^{(m)} = B$ . In addition, the carrier frequency still follows (13) but  $\Delta f^{(m)}$  now satisfies:

$$\begin{cases} \Delta f^{(0)} = -\frac{B}{2} + \frac{B_p^{(0)}}{2} \\ \Delta f^{(m)} = -\frac{B}{2} + \sum_{l=0}^{m-1} B_p^{(l)} + \frac{B_p^{(m)}}{2} \text{ for } m = 1, \dots, N_p - 1 \end{cases} \quad (16)$$

The so-called "variable chirp-rate SF-LFM waveform" is defined by the set of the pulse bandwidths  $\{B_p^{(m)}\}_{m=0, \dots, N_p-1}$  and of the pulse durations  $\{T_p^{(m)}\}_{m=0, \dots, N_p-1}$ .

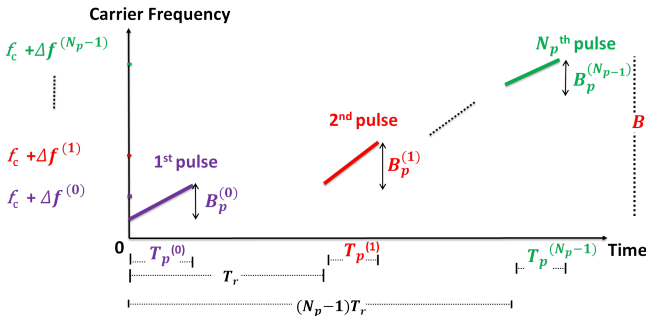


Figure 3: Stepped frequency linear frequency modulated waveform with variable chirp rate

In the next section, let us see how to generate it from an NLFM waveform.

### 3.2. At the transmitter part

Let us first present some details of the different steps done at the transmitter.

1. **From the SC tangent-based NLFM waveform to its linear piece-wise approximation:** Let us consider a tangent-based NLFM waveform whose instantaneous frequency satisfies:

$$f_{tan}(t) = f\left(t - \frac{T_p}{2}\right) + \frac{B}{2} \quad (17)$$

where  $f(t)$  is defined in (2). This instantaneous frequency is illustrated in Fig. 4a.

**Remark:** while  $f(t)$  satisfies  $f(t) + f(-t) = 0$  since its an odd function,  $f_{tan}$  has the following property:

$$\begin{aligned} f_{tan}(t) - \frac{B}{2} &= f\left(t - \frac{T_p}{2}\right) \underset{f(t) \text{ odd}}{=} -f\left(-t + \frac{T_p}{2}\right) \\ &\underset{(17)}{=} -(f_{tan}(-t + T_p) - \frac{B}{2}) \end{aligned} \quad (18)$$

Consequently, one has:

$$f_{tan}(t) + f_{tan}(T_p - t) = B \quad (19)$$

In order to derive the parameters of our waveform, we first suggest approximating  $f_{tan}(t)$  by a linear piece-wise function. We could select the time instants between 0 and  $T_p$ , but as the tangent-based NLFM waveform is odd with respect to  $\frac{T_p}{2}$ , we suggest selecting the time instants between 0 and  $\frac{T_p}{2}$ . Then, the time instants between  $\frac{T_p}{2}$  and  $T_p$  as well as the corresponding instantaneous frequencies can be deduced so that the anti-symmetry is maintained. Thus, at different time instants denoted as  $\{0 \leq \tau_m \leq \frac{T_p}{2}\}_{m=0, \dots, N+1}$ , the instantaneous frequency takes the values  $\{0 \leq \nu_m \leq \frac{B}{2}\}_{m=0, \dots, N+1}$  and coincides with  $f_{tan}(t)$  as follows:

$$\begin{cases} (\tau_0, \nu_0) = (0, 0) \\ (\tau_{N+1}, \nu_{N+1}) = (\frac{T_p}{2}, \frac{B}{2}) \\ \nu_m = f_{tan}(\tau_m) = f\left(\tau_m - \frac{T_p}{2}\right) + \frac{B}{2} \\ \text{for } m = 0, \dots, N+1 \end{cases} \quad (20)$$

where  $f(t)$  is given in (2).

For  $\frac{T_p}{2} \leq t \leq T_p$ , using (19), the time instants and the corresponding instantaneous frequencies are then given by:

$$\begin{cases} (\tau_{2N+2}, \nu_{2N+2}) = (T_p, B) \\ \tau_m = T_p - \tau_{2N+2-m} \text{ for } m = N+2, \dots, 2N+2 \\ \nu_m = f_{tan}(\tau_m) = B - \nu_{2N+2-m} \end{cases} \quad (21)$$

Therefore, the number of couples of parameters required to define a SC-PW-NLFM waveform can be reduced to  $N+2$ , namely  $\{(\tau_m, \nu_m)\}_{m=0, \dots, N+1}$ . Using (20) and (21), the SC tangent-based NLFM waveform can be approximated by a SC-PW-NLFM waveform as illustrated in Fig. 4.b.

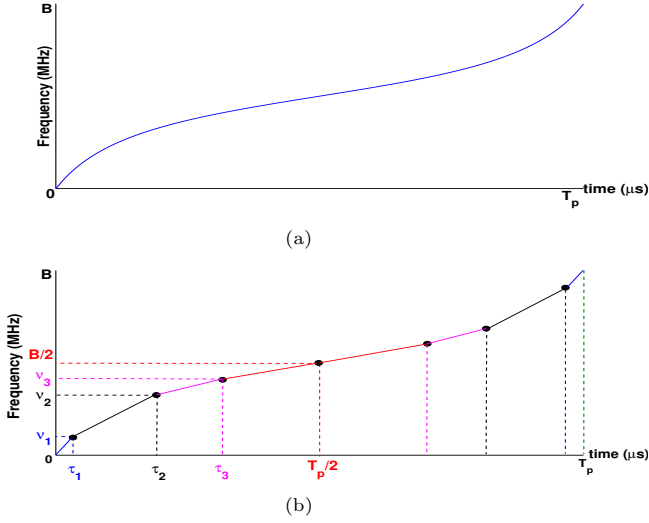


Figure 4: Instantaneous frequency of the (a) tangent-based NLFM waveform with  $\beta = 1.21$  (b) SC-PW-NLFM waveform.

## 2. From the SC-PW-NLFM to the expression of the transmitted waveform:

To get the expression of the proposed waveform, the parameters in (20) and (21) are used to define a train of  $N_p$  baseband LFM pulses with different chirp rates and durations. As illustrated in Fig. 4b, the two pieces around  $\frac{T_p}{2}$  have the same duration and bandwidth. Two possibilities can hence be considered to define the pulses of the proposed waveform from the SC-PW-NLFM waveform: On the hand, the two pieces around  $\frac{T_p}{2}$  can be used to generate two pulses of the proposed waveform. In this case,  $N_p = 2N + 2$ .

On the other hand, the two pieces are combined to represent a single pulse with a duration and a bandwidth equal to twice that of one piece. In this case,  $N_p = 2N + 1$ .

In the following, we will focus our attention on an approximation where the first possibility is considered. There is no particular piece in this case and there is the same number of pieces characterizing the intervals  $[0, \frac{T_p}{2}]$  and  $[\frac{T_p}{2}, T_p]$ . This also follows the definition of a train of a piecewise linear functions given in [10]. Thus, the  $N_p$  LFM baseband pulses shown in Fig. 5a can be modeled for  $m = 0, \dots, 2N + 1$  as:

$$s_{bb,m}(t) = \text{rect}\left(\frac{1}{\tau_{m+1} - \tau_m}(t - mT_r - \frac{\tau_{m+1} - \tau_m}{2})\right) \times \exp\left(j\pi\gamma^{(m)}(t - mT_r - \frac{\tau_{m+1} - \tau_m}{2})^2\right) \quad (22)$$

where the term  $mT_r - \frac{\tau_{m+1} - \tau_m}{2}$  is required in the *rect* function to focus on the interval  $[mT_r, mT_r + \tau_{m+1} - \tau_m]$ . It is also required in the complex exponential to have a spectrum centered around zero.

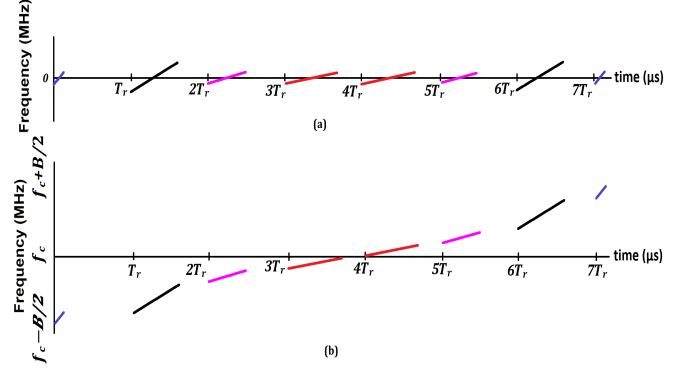


Figure 5: Instantaneous frequency of the (a) train of baseband chirp pulses (b) transmitted variable chirp rate SF-LFM waveform with center frequency  $f_c$

In addition, according to (21), the durations of the  $(m+1)^{th}$  and the  $(2N+2-m)^{th}$  pulses are the same for  $m = 0, \dots, N$ . So, one has:

$$\begin{cases} T_p^{(m)} = \tau_{m+1} - \tau_m & \text{for } m = 0, \dots, N \\ T_p^{(m)} = T_p^{(2N-m+1)} & \text{for } m = N + 1, \dots, 2N + 1 \end{cases} \quad (23)$$

The bandwidth  $B_p^{(m)}$  of the  $(m+1)^{th}$  pulse is defined as follows:

$$\begin{cases} B_p^{(m)} = \nu_{m+1} - \nu_m & \text{for } m = 0, \dots, N \\ B_p^{(m)} = B_p^{(2N-m+1)} & \text{for } m = N + 1, \dots, 2N + 1 \end{cases} \quad (24)$$

Finally, the chirp rate of the  $(m+1)^{th}$  pulse is given by:

$$\begin{cases} \gamma^{(m)} = \frac{B_p^{(m)}}{T_p^{(m)}} & \text{for } m = 0, \dots, N \\ \gamma^{(m)} = \gamma^{(2N-m+1)} & \text{for } m = N + 1, \dots, 2N + 1 \end{cases} \quad (25)$$

Afterward, the whole train is frequency translated to the carrier frequency  $f_c$ , as shown in Fig. 5b. This is done by multiplying  $s_{bb,m}(t)$  with the proper exponential term. For the  $(m+1)^{th}$  pulse ( $m \in \llbracket 0, 2N+1 \rrbracket$ ), the proposed transmitted waveform can be expressed as follows:

$$s_{tx,m}(t) = s_{bb,m}(t) \exp(j2\pi f_c^{(m)} t) \quad (26)$$

where  $f_c^{(m)} = f_c + \Delta f^{(m)}$  and  $\Delta f^{(m)}$  is defined in (16).

By combining (22), (23) and (26), the transmitted waveform can be expressed in a detailed manner as follows:

$$s_{tx,m}(t) = \text{rect}\left(\frac{1}{T_p^{(m)}}(t - mT_r - \frac{T_p^{(m)}}{2})\right) \exp\left(j2\pi\left(\frac{\gamma^{(m)}}{2}(t - mT_r - \frac{T_p^{(m)}}{2})^2 + (f_c + \Delta f^{(m)})t\right)\right) \quad (27)$$

In the next section, let us analyze how the receiver part is organized.

### 3.3. At the receiver part

#### 3.3.1. Introduction

In order to process the back-scattered received echoes in the time domain, there exists a well-defined algorithm in the literature called the TD algorithm [5]. However, the latter deals with a train of pulses having a constant chirp rate, with constant pulse-width and bandwidth, which is not the case in this paper. Thus, we suggest exploiting a generalized version of the TD algorithm. It aims at reconstructing a wide-band NLFM waveform by coherently combining an ensemble of variable narrow-bandwidth chirp waveforms in the time domain. The resulting time-frequency relationship of the reconstructed waveform is equivalent to a baseband version of the wideband SC-PW-NLFM waveform similar to the one shown in Fig. 4 but centered at zero Hz.

Concerning the steps of the TD algorithm at the receiver, it should be noted that they are applied to each range window<sup>3</sup> separately. The latter may correspond to more than one scatterer as shown in Fig. 6. For the sake of simplicity, each range window is assumed to correspond to one scatterer in the sequel.

At the receiver, three aspects have to be addressed:

- How to guarantee the phase continuity when reconstructing the waveform.
- How to address the phase continuity problem in the discrete-time domain.
- How to optimize the receiver part in terms of reducing the sampling frequency.

Directly presenting the final algorithm taking into account these three aspects could not be clear enough for the reader. For this reason, the remainder of this section is organized as follows: in section 3.3.2, we illustrate how the signal would be processed in the continuous-time domain to maintain the phase continuity. Then, in section 3.3.3, the TD algorithm is presented where the last two issues are addressed.

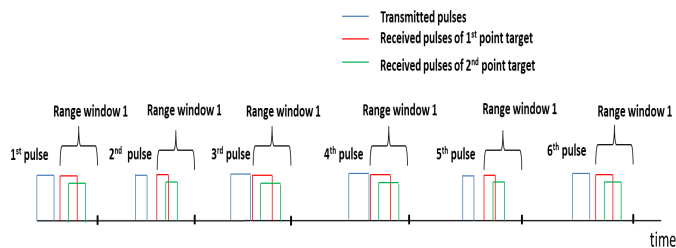


Figure 6: Transmitted and received pulses over one range window

<sup>3</sup>It represents the range over which the received echoes are collected and processed.

#### 3.3.2. Preamble: processing steps that would be done if the signal was only processed in the continuous-time domain

Our purpose is to present how the waveform would be reconstructed if the signal was only processed in the continuous-time domain. In this case, the main issue to be addressed is to guarantee the phase continuity of the pulses at the receiver.

At the receiver, the signal can be formulated as follows:

$$s_{rx,m}(t) = \alpha_m s_{tx,m}(t - t_d) + n(t) \quad (28)$$

where  $\alpha_m$  and  $n(t)$  respectively denote the  $(m+1)^{th}$  channel attenuation coefficient associated with the  $(m+1)^{th}$  pulse, and the additive measurement white Gaussian noise. In the sequel,  $\alpha_m = 1$  is considered because the burst that consists of  $2N+2$  pulses is assumed to be transmitted during the CPI, hence it is subject to the same channel effect. Furthermore, to ease the grasp of the steps of our algorithm, we will focus on the signal part only. This amounts to addressing the ideal case.

Subsequently, the "ideal" received  $(m+1)^{th}$  pulse is down converted to baseband, as shown in Fig. 7a. This is done by multiplying the received  $(m+1)^{th}$  pulse with the appropriate sinusoidal signal as follows:

$$\begin{aligned} s_{rx,bb,m}(t) &\stackrel{(28)}{=} s_{tx,m}(t - t_d) \exp(-j2\pi f_c^{(m)} t) \\ &\stackrel{(26)}{=} s_{bb,m}(t - t_d) \exp(-j2\pi f_c^{(m)} t_d) \end{aligned} \quad (29)$$

This amounts to saying that:

$$\begin{aligned} s_{rx,bb,m}(t) &= \text{rect}\left(\frac{1}{T_p^{(m)}}\left(t - mT_r - \frac{T_p^{(m)}}{2} - t_d\right)\right) \\ &\times \exp\left(j2\pi\left(\frac{\gamma^{(m)}}{2}\left(t - mT_r - \frac{T_p^{(m)}}{2} - t_d\right)^2 - f_c^{(m)} t_d\right)\right) \end{aligned} \quad (30)$$

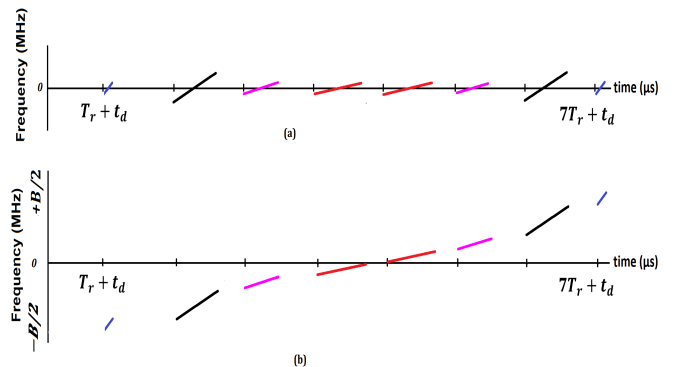


Figure 7: Instantaneous frequency of (a) the train of received baseband chirp pulses (b) the train of received chirp pulses shifted in frequency

Then, we suggest frequency shifting each pulse to its proper position, as shown in Fig. 7b. This is done by multiplying each pulse by the proper exponential factor as follows:

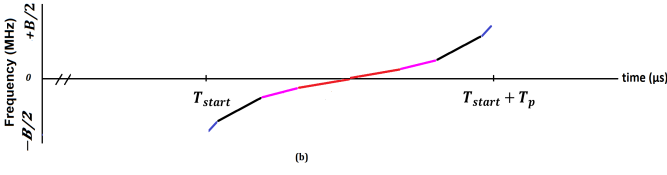


Figure 8: Instantaneous frequency of the reconstructed SC-PW-NLFM waveform

$$s_{rx,bb,m}^{fshift}(t) = s_{rx,bb,m}(t) \exp(j2\pi \Delta f^{(m)} t) \quad (31)$$

Using (30) and (31) and rearranging some terms, one can rewrite the  $m^{\text{th}}$  frequency-shifted received pulse as follows:

$$\begin{aligned} s_{rx,bb,m}^{fshift}(t) &= \text{rect}\left(\frac{1}{T_p^{(m)}}(t - mT_r - \frac{T_p^{(m)}}{2} - t_d)\right) \quad (32) \\ &\times \exp\left(j2\pi\left(\frac{\gamma^{(m)}}{2}(t - mT_r - \frac{T_p^{(m)}}{2} - t_d)^2\right.\right. \\ &\left.\left. + \Delta f^{(m)}(t - mT_r - \frac{T_p^{(m)}}{2} - t_d)\right)\right) \\ &\times \exp(-j2\pi f_c t_d) \exp(j2\pi \Delta f^{(m)}(mT_r + \frac{T_p^{(m)}}{2})) \end{aligned}$$

By introducing:

$$\phi_{rx,bb,m}^{shift}(t) = 2\pi\left(\frac{\gamma^{(m)}}{2}t^2 + \Delta f^{(m)}t\right) \quad (33)$$

the above signal can be rewritten as follows:

$$\begin{aligned} s_{rx,bb,m}^{fshift}(t) &= \text{rect}\left(\frac{1}{T_p^{(m)}}(t - mT_r - \frac{T_p^{(m)}}{2} - t_d)\right) \quad (34) \\ &\times \exp\left(j\phi_{rx,bb,m}^{shift}(t - mT_r - \frac{T_p^{(m)}}{2} - t_d)\right) \\ &\times \exp(-j2\pi f_c t_d) \exp(j2\pi \Delta f^{(m)}(mT_r + \frac{T_p^{(m)}}{2})) \end{aligned}$$

Given the set of received pulses that have been frequency-shifted, the purpose is now to reconstruct the whole waveform. The reconstructed waveform can start at a time  $T_{start}$ , as shown in Fig. 8. Moreover, the time shifts cannot depend on  $t_d$  for two reasons:  $t_d$  is unknown and the delay lines that will be used to time-shift the signals are pre-defined and cannot be adjusted to  $t_d$ . Thus, we could consider that the reconstruction of the waveform starts  $T_w$  seconds after receiving the last pulse. This means that:

$$T_{start} = (2N + 1)T_r + T_p - \tau_{2N+1} + t_d + T_w \quad (35)$$

In this case, as the first pulse has to start at time  $T_{start}$ , it has to be time-shifted by:

$$\begin{aligned} \delta t_0 &= T_{start} - t_d \quad (36) \\ &\stackrel{(35)}{=} (2N + 1)T_r + T_p - \tau_{2N+1} + T_w \end{aligned}$$

More generally, the  $(m + 1)^{\text{th}}$  pulse has to start at time  $\tau_m$  and hence must be time-shifted by:

$$\begin{aligned} \delta t_m &= T_{start} + \tau_m - (mT_r + t_d) \quad (37) \\ &\stackrel{(35)}{=} (2N + 1 - m)T_r + T_p + \tau_m - \tau_{2N+1} + T_w \end{aligned}$$

Given (37), the time-shifted pulses can be written as:

$$\begin{aligned} s_{rx,bb,m}^{tshift}(t) &= \text{rect}\left(\frac{1}{T_p^{(m)}}(t - mT_r - \delta t_m - \frac{T_p^{(m)}}{2} - t_d)\right) \quad (38) \\ &\exp\left(j\phi_{rx,bb,m}^{fshift}(t - mT_r - \delta t_m - \frac{T_p^{(m)}}{2} - t_d)\right) \\ &\times \exp(-j2\pi f_c t_d) \exp(j2\pi \Delta f^{(m)}(mT_r + \frac{T_p^{(m)}}{2})) \end{aligned}$$

or, equivalently:

$$\begin{aligned} s_{rx,bb,m}^{tshift}(t) &= \text{rect}\left(\frac{1}{T_p^{(m)}}\left(t - (T_{start} + \tau_m + \frac{T_p^{(m)}}{2})\right)\right) \quad (39) \\ &\exp\left(j\phi_{rx,bb,m}^{fshift}(t - (T_{start} + \tau_m + \frac{T_p^{(m)}}{2}))\right) \\ &\times \exp(-j2\pi f_c t_d) \exp(j2\pi \Delta f^{(m)}(mT_r + \frac{T_p^{(m)}}{2})) \end{aligned}$$

In order to reconstruct the SC-PW waveform, a continuity in the phases of the pulses should be guaranteed before adding them. For this purpose, one just has to express  $s_{rx,bb,m}^{tshift}(T_{start} + \tau_{m+1})$  and  $s_{rx,bb,m+1}^{tshift}(T_{start} + \tau_{m+1})$ . At these time instants, the  $\text{rect}$  function is always equal to 1. Moreover,  $\exp(-j2\pi f_c t_d)$  does not play a role for the continuity as it appears for each time interval. Therefore, the continuity must be guaranteed between:

$$\begin{aligned} &\exp\left(j\phi_{rx,bb,m}^{fshift}(T_{start} + \tau_{m+1} - (T_{start} + \tau_m + \frac{T_p^{(m)}}{2}))\right) \quad (40) \\ &\times \exp(j2\pi \Delta f^{(m)}(mT_r + \frac{T_p^{(m)}}{2})) \end{aligned}$$

and

$$\begin{aligned} &\exp\left(j\phi_{rx,bb,m+1}^{fshift}(T_{start} + \tau_{m+1} - (T_{start} + \tau_{m+1} + \frac{T_p^{(m+1)}}{2}))\right) \quad (41) \\ &\times \exp(j2\pi \Delta f^{(m+1)}((m + 1)T_r + \frac{T_p^{(m+1)}}{2})) \end{aligned}$$

Given (33), let us express the phases of both terms:

$$\begin{aligned} &\phi_{rx,bb,m}^{shift}\left(\frac{T_p^{(m)}}{2}\right) + 2\pi \Delta f^{(m)}(mT_r + \frac{T_p^{(m)}}{2}) \quad (42) \\ &= 2\pi \left[ \frac{\gamma^{(m)}}{2} \left(\frac{T_p^{(m)}}{2}\right)^2 + \Delta f^{(m)}(mT_r + \frac{T_p^{(m)}}{2}) \right] \end{aligned}$$

and

$$\begin{aligned} &\phi_{rx,bb,m+1}^{fshift}\left(-\frac{T_p^{(m+1)}}{2}\right) + 2\pi \Delta f^{(m+1)}((m + 1)T_r + \frac{T_p^{(m+1)}}{2}) \quad (43) \\ &= 2\pi \left[ \frac{\gamma^{(m+1)}}{2} \left(\frac{T_p^{(m+1)}}{2}\right)^2 + (m + 1)T_r \Delta f^{(m+1)} \right] \end{aligned}$$

Let us start with the first case, *i.e.*  $m = 0$ . This leads to:

$$\begin{aligned} \phi_{rx,bb,0}^{fshift}\left(\frac{T_p^{(0)}}{2}\right) + 2\pi\Delta f^{(0)}\frac{T_p^{(0)}}{2} \\ = 2\pi\left[\frac{\gamma^{(0)}}{2}\left(\frac{T_p^{(0)}}{2}\right)^2 + \Delta f^{(0)}T_p^{(0)}\right] \end{aligned} \quad (44)$$

and

$$\begin{aligned} \phi_{rx,bb,1}^{fshift}\left(-\frac{T_p^{(1)}}{2}\right) + 2\pi\Delta f^{(1)}\left(T_r + \frac{T_p^{(1)}}{2}\right) \\ = 2\pi\left[\frac{\gamma^{(1)}}{2}\left(\frac{T_p^{(1)}}{2}\right)^2 + \Delta f^{(1)}T_r\right] \end{aligned} \quad (45)$$

Let us introduce a phase compensation  $u_1$  so that:

$$\begin{aligned} \phi_{rx,bb,0}^{fshift}\left(\frac{T_p^{(0)}}{2}\right) + 2\pi\Delta f^{(0)}\frac{T_p^{(0)}}{2} \\ = \phi_{rx,bb,1}^{fshift}\left(-\frac{T_p^{(1)}}{2}\right) + 2\pi\Delta f^{(1)}\left(T_r + \frac{T_p^{(1)}}{2}\right) + 2\pi u_1 \end{aligned} \quad (46)$$

This means that  $s_{rx,bb,1}^{tshift}(t)$  is multiplied by  $exp(j2\pi u_1 t)$ . By combining the three equations written above, one can deduce  $u_1$ .

$$u_1 = -\frac{\gamma^{(1)}}{2}\left(\frac{T_p^{(1)}}{2}\right)^2 - \Delta f^{(1)}T_r + \frac{\gamma^{(0)}}{2}\left(\frac{T_p^{(0)}}{2}\right)^2 + \Delta f^{(0)}T_p^{(0)} \quad (47)$$

More generally, one has:

$$\begin{cases} u_0 = 0 \\ u_m = u_{m-1} - \frac{\gamma^{(m)}}{2}\left(\frac{T_p^{(m)}}{2}\right)^2 - m\Delta f^{(m)}T_r \\ \quad + \frac{\gamma^{(m-1)}}{2}\left(\frac{T_p^{(m-1)}}{2}\right)^2 + \Delta f^{(m-1)}((m-1)T_r + T_p^{(m-1)}) \\ \quad \text{for } 1 \leq m \leq 2N+1 \end{cases} \quad (48)$$

At this stage, the reconstructed waveform would be processed by a MF in order to produce the HRRP.

So far, the signal processing steps have been illustrated in the continuous-time domain. In the sequel, the way to process the signal in the discrete-time domain is presented. In this case, two problems have to be addressed when designing the TD algorithm: How to use a small sampling frequency? How to use a discrete-time signal while preserving the continuity of the phases?

### 3.3.3. Processing steps in the discrete-time domain

In this section, the processing steps in the discrete domain are presented. Instead of directly sampling the received signal at a sampling frequency equal to  $B$  Hz, we propose to operate in two steps: sampling at a lower rate and then interpolating. The advantage of the proposed processing chain over the one used for the SC-PW-NLFM waveform is to avoid a high sampling frequency thanks to the SF methodology used. The steps of the TD algorithm depicted in Fig. 9 can be summarized as follows:

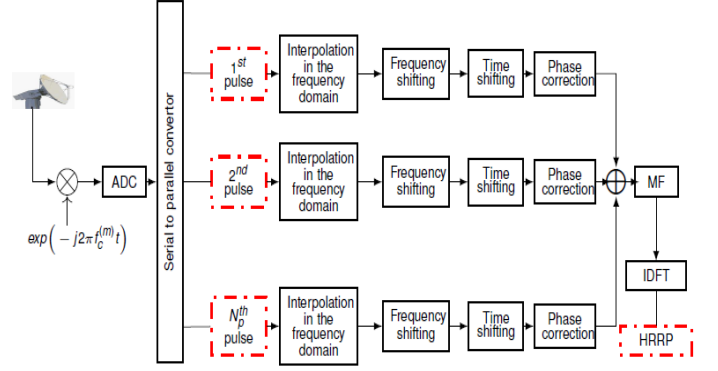


Figure 9: Steps of the generalized TD algorithm

1. For each received pulse, sample the baseband signals whose expression is given in (29) by using the sampling frequency that satisfies:

$$F_s^{(Rx)} = \frac{1}{T_s^{(Rx)}} = \frac{B}{\eta} \quad (49)$$

where  $\eta$  is defined by:

$$\eta = \left\lceil \frac{B}{2 \max_{0 \leq m \leq N+1} B_p^{(m)}} \right\rceil \quad (50)$$

This means for instance that:

$$\eta = 2 \text{ if } \frac{B}{6} < \max_{0 \leq m \leq N+1} B_p^{(m)} \leq \frac{B}{4} \quad (51)$$

In this case, the number of samples that represent each pulse is equal to  $\lfloor F_s^{(Rx)} T_p^{(m)} \rfloor$ . If  $F_s^{(Rx)} T_p^{(m)}$  is not an integer, the duration of the pulse cannot be retrieved exactly and hence must be approximated. Thus, the truncated duration and bandwidth of the  $(m+1)^{th}$  sampled received pulse must be considered and are respectively denoted as:

$$T_{p,trn}^{(m)} = \frac{\lfloor F_s^{(Rx)} T_p^{(m)} \rfloor}{F_s^{(Rx)}} \quad (52)$$

and

$$\begin{cases} B_{trn}^{(m)} = \nu_{m+1,trn} - \nu_m \text{ for } m = 0, \dots, N \\ B_{trn}^{(m)} = B_{trn}^{(2N-m+1)} \text{ for } m = N+1, \dots, 2N+1 \end{cases} \quad (53)$$

where  $\nu_{m+1,trn} = f_{tan}(\tau_{m+1,trn})$  and  $\tau_{m+1,trn}$  is defined as:

$$\begin{cases} \tau_{0,trn} = 0 \\ \tau_{m+1,trn} = \tau_m + T_{p,trn}^{(m)} \text{ for } m = 0, \dots, N \end{cases} \quad (54)$$

It should be noted that (52) and (54) will be used in the following steps when  $F_s^{(Rx)} T_p^{(m)}$  is not integer

to avoid any problem in the reconstruction of the HRRP.

Then, for the sake of simplicity, let us address the example where the delay is strictly a multiple of the sampling period, at the receiver, *i.e.*:

$$t_d = dT_s^{(Rx)} \quad (55)$$

Hence, using (26), (29) becomes for  $n \in \llbracket 0, L_m - 1 \rrbracket$  with  $L_m = \lfloor T_p^{(m)} F_s^{(Rx)} \rfloor$ :

$$s_{rx,bb,m}(n) = s_{bb,m}((n-d)T_s^{(Rx)}) \exp(-j2\pi f_c^{(m)} dT_s^{(Rx)}) \quad (56)$$

- Interpolate  $s_{rx,bb,m}(n)$  so that the new sampling frequency becomes:

$$F_s^{(int)} = \frac{1}{T_s^{(int)}} = B = \eta F_s^{(Rx)} \quad (57)$$

where  $T_s^{(int)}$  denotes the new sampling time. This can be done either in the time domain or in the frequency domain<sup>4</sup>. The resulting signal is denoted  $s_{rx,bb,m}^{int}(n)$  for  $n \in \llbracket 0, \eta L_m - 1 \rrbracket$ . Sampling at  $F_s^{(Rx)}$  and then interpolating the received signal instead of directly sampling it at the sampling frequency  $B$  makes it possible to use a cheap ADC.

**Remark:** For a proper interpolation of  $s_{rx,bb,m}(n)$ ,  $L_m$  should be greater than 2. Thus, the minimum duration between any two consecutive time instants should be greater than a certain threshold denoted by  $\epsilon$ . For any  $m \in \llbracket 0, N - 1 \rrbracket$ , this leads to:

$$T_{p,trn}^{(m)} \geq T_p^{(m)} \geq \epsilon = \frac{2}{F_s^{(Rx)}} \quad (58)$$

- Frequency-shift each pulse to its proper position so that it occupies a frequency band shifted by  $-\frac{B}{2}$  Hz compared with its corresponding one, the SC-PW-NLFM waveform shown in Fig. 4. This is done by multiplying each pulse by the proper exponential factor as follows:

$$s_{rx,bb,m}^{int,shift}(n) = s_{rx,bb,m}^{int}(n) \exp(j2\pi \Delta f^{(m)} n T_s^{(int)}) \quad (59)$$

where  $\Delta f^{(m)}$  is defined in (16). When  $F_s^{(Rx)} T_p^{(m)}$  is not integer,  $\Delta f^{(m)}$  satisfies:

$$\begin{cases} \Delta f^{(0)} &= -\frac{B}{2} + \frac{B_{p,trn}^{(0)}}{2} \\ \Delta f^{(m)} &= -\frac{B}{2} + \sum_{l=0}^{m-1} B_{p,trn}^{(l)} + \frac{B_{p,trn}^{(m)}}{2} \\ &\text{for } m = 1, \dots, N_p - 1 \end{cases} \quad (60)$$

<sup>4</sup>In the former, the signal is upsampled by a factor equal to  $\eta$  and then interpolated by using a low-pass finite-impulse response (FIR) filter. Polyphase filters are often considered. As for the latter, the discrete Fourier transform (DFT) of  $s_{rx,bb,m}$  is decomposed into two parts. Zeros are then introduced in between to obtain a sequence of length  $\eta T_m$ . Then the real part of the inverse DFT is computed.[32]

- Time-shift the result obtained for each pulse in (59) by  $\delta t_m$  defined in (37). When  $F_s^{(Rx)} T_p^{(m)}$  is not integer,  $\delta t_m$  now satisfies:

$$\delta t_m = (2N + 1 - m)T_r + T_p + \tau_{m,trn} - \tau_{2N+1} + T_w \quad (61)$$

- Add a phase correction term to each pulse to avoid any phase discontinuity in the reconstructed SC-PW-NLFM waveform. It is done by multiplying (59) with an appropriate exponential term, as follows:

$$s_{rx,bb,m}^{int,shift,pc}(n) = s_{rx,bb,m}^{int,shift}(n) \exp(j2\pi u_m n) \quad (62)$$

where  $u_m$  is defined in (48). When  $F_s^{(Rx)} T_p^{(m)}$  is not integer,  $u_m$  satisfies:

$$\begin{cases} u_0 &= 0 \\ u_m &= u_{m-1} - \frac{\gamma^{(m)}}{2} (T_{p,trn}^{(m-1)} - \frac{T_p^{(m)}}{2})^2 - m \Delta f^{(m)} T_r \\ &\quad + \frac{\gamma^{(m-1)}}{2} (\frac{T_p^{(m-1)}}{2})^2 \\ &\quad + \Delta f^{(m-1)} ((m-1)T_r + T_{p,trn}^{(m-1)}) \\ &\text{for } 1 \leq m \leq 2N + 1 \end{cases} \quad (63)$$

- Add the obtained pulses together. The reconstructed waveform denoted as  $s_{rx}^{SC-PW-NLFM}(n T_s^{(int)} - d T_s^{(int)})$ , is a delayed discrete baseband version of a SC-PW-NLFM waveform. Its instantaneous frequency is similar<sup>5</sup> to the one given in Fig. 4.b, but its spectral components are centered around the zero-component instead of  $\frac{B}{2}$ .
- Apply a MF in the frequency domain to the reconstructed waveform. It consists in applying a DFT to  $s_{rx}^{SC-PW-NLFM}(n T_s^{(int)} - d T_s^{(int)})$  after padding it with  $\eta L_m - 1$  zeros.

Then, multiply the result by  $\overline{S_{tx,bb}^{SC-PW-NLFM}(k)}$ , where  $\overline{(\cdot)}$  denotes the conjugate,  $S_{tx,bb}^{SC-PW-NLFM}(k)$  is the DFT of  $s_{tx,bb,pad}^{SC-PW-NLFM}(n)$ . The sequence  $s_{tx,bb,pad}^{SC-PW-NLFM}(n)$  is a padded version of  $s_{tx,bb}^{SC-PW-NLFM}(n)$  with  $\eta L_m - 1$  zeros. Thus, the obtained result can be written for  $k \in \llbracket 0, 2\eta L_m - 2 \rrbracket$  as:

$$Z(k) = |S_{tx,bb}^{SC-PW-NLFM}(k)|^2 \exp\left(-j2\pi \frac{k}{2\eta L_m - 1} \frac{2R}{c}\right) \quad (64)$$

- Produce the HRRP by applying an inverse DFT to (64).

In this section, the processing chain from the transmitter to the receiver has been presented. Nevertheless, the performance is not optimized in terms of PSLR, ISLR, and range resolution. The latter are mainly related to the selection of the parameters of the waveform, namely the time instants  $\{\tau_m\}_{m=1,\dots,N}$ . In the following, we present two ways to choose them by using genetic algorithms.

<sup>5</sup>few approximations may exist due to the segment truncations

## 4. Optimizing the parameters of the proposed waveform

### 4.1. Introduction

The performance in terms of PSLR, ISLR, and range resolution of the proposed waveform depend on the set of parameters  $\{(\tau_m, \nu_m)\}_{m=1, \dots, N}$ . Our purpose is to select the parameters that lead to the closest performance to that of the tangent-based NLFM waveform. As the set of frequencies  $\{\nu_m\}_{m=1, \dots, N+1}$  can be deduced from the set of time instants  $\{\tau_m\}_{m=1, \dots, N+1}$  by using (20), only  $\{\tau_m\}_{m=1, \dots, N}$  have to be optimized.

For this purpose, a multi-objective optimization problem can be considered. It can take into account the performance of the processing chain in terms of PSLR, ISLR, and range resolution. In this optimization problem, we suggest considering the following three criteria:

$$F_{PSLR}(\underline{x}) = \left| \frac{PSLR(\underline{x}) - PSLR_{ref}}{PSLR_{ref}} \right| \quad (65)$$

$$F_{ISLR}(\underline{x}) = \left| \frac{ISLR(\underline{x}) - ISLR_{ref}}{ISLR_{ref}} \right| \quad (66)$$

and

$$F_{R_{res}}(\underline{x}) = \left| \frac{R_{res}(\underline{x}) - R_{res,ref}}{R_{res,ref}} \right| \quad (67)$$

where  $\underline{x}$  denotes the vector storing the time instants  $\{\tau_m\}_{m=1, \dots, N}$ .  $PSLR(\underline{x})$ ,  $ISLR(\underline{x})$ , and  $R_{res}(\underline{x})$  are respectively the PSLR, the ISLR, and the range resolution obtained when using the waveform parameters  $\underline{x}$ . In addition,  $PSLR_{ref}$ ,  $ISLR_{ref}$ , and  $R_{res,ref}$  are respectively the ISLR, the PSLR, and the range resolution of the tangent-based NLFM waveform for a specific value of  $\beta$ .

In this paper, two approaches are considered to address the multi-objective optimization issue. The first one consists in minimizing a single fitness function that consists of a weighted sum of the three above criteria whereas the second one consists in addressing the multi-objective problem by considering the Pareto front. Both approaches are based on genetic algorithms (GAs). GA is a stochastic global search optimization technique based on the principle of genetics and natural selection [33]. It has been extensively used as a search and optimization tool in many fields including sciences, manufacturing, and engineering [34] [35]. GA is an iterative process. It starts with an initial population consisting of a certain number of candidates. The relevance of each candidate is evaluated according to a fitness function. Then, new solutions are generated using selection, crossover, and mutation operators. In the following, both methods are presented.

### 4.2. First GA-based approach using a single fitness function

In this section, we consider using the standard GA for minimizing a single fitness function that consists of a

weighted sum of the three criteria defined in the previous section. The latter is given by:

$$F(\underline{x}) = (1 - \lambda_1 - \lambda_2)F_{PSLR}(\underline{x}) + \lambda_1 F_{ISLR}(\underline{x}) + \lambda_2 F_{R_{res}}(\underline{x}) \quad (68)$$

where  $0 \leq \lambda_1 \leq 1$  and  $0 \leq \lambda_2 \leq 1 - \lambda_1$  are the weights. These weights can be adjusted by the practitioner. This depends on the environment and the type of targets to be detected. If the purpose is to detect targets with small RCS in the presence of targets with high RCS, a greater level of importance should be given to the PSLR. However, if the goal is to detect targets in the presence of distributed clutter, a greater level of importance should be given to the ISLR. Similarly, if the scenario of operation requires high range resolution, a greater level of importance should be given to  $R_{res}$ . To take into account the fact that there is a constraint on the minimum duration between any two consecutive time instants (See (58) in section 3.3) we operate as follows:

- Generation of the initial population: As  $\tau_0 = 0$  and  $\tau_{N+1} = \frac{T_p}{2}$ , the initial population is generated so that for  $m \in \llbracket 0, N-1 \rrbracket$ , the time instants satisfy:

$$\tau_m + \epsilon < \tau_{m+1} < \frac{T_p}{2} - (N - m)\epsilon$$

where  $\epsilon$  was introduced in (58).

As a consequence, the initial population corresponds to a set of  $Q_p$  vectors of size  $N$ .

- Selection: It consists in randomly selecting two vectors, namely  $\underline{C}_i^f = [\tau_1^f, \tau_2^f, \dots, \tau_{k-1}^f, \tau_k^f, \dots, \tau_N^f]$  and  $\underline{C}_i^m = [\tau_1^m, \tau_2^m, \dots, \tau_{k-1}^m, \tau_k^m, \dots, \tau_N^m]$  from the population at the  $i^{th}$  generation.
- Crossover: After using the single-point crossover, the resulting candidates, called children, are:

$$\underline{C}_1 = [\tau_1^f, \tau_2^f, \dots, \tau_{k-1}^f, \tau_k^m, \dots, \tau_N^m] \quad (69)$$

$$\underline{C}_2 = [\tau_1^m, \tau_2^m, \dots, \tau_{k-1}^m, \tau_k^f, \dots, \tau_N^f] \quad (70)$$

The time instants of one of the obtained candidates necessarily respect the constraint. Thus, if  $\tau_k^m - \tau_{k-1}^f > \epsilon$ ,  $\underline{C}_1$  is chosen. Otherwise,  $\underline{C}_2$  is kept. Before belonging to the population of candidate vectors at the  $(i+1)^{th}$  iteration, a mutation will be done on the chosen child vector.

**Remark:** When  $N$  is equal to 1, the above crossover cannot be applied. Therefore, we suggest using a linear crossover. In this case, the child is defined as follows:

$$\underline{C}_1 = \frac{1}{2}\underline{C}_i^f + \frac{1}{2}\underline{C}_i^m \quad (71)$$

- Mutation: Let us assume that  $\underline{C}_1$  was chosen by the crossover operator. We suggest mutating each element, or equivalently each time instant, of  $\underline{C}_1$  separately in a way that guarantees that the resulting

candidate respects the constraint (58). It is done as follows:

The mutations on the time instants are done successively. Let us start with the first time instant  $\underline{C}_1(1)$ . A random number  $r$  uniformly distributed between 0 and 1 is drawn. If  $r$  is smaller than the probability of mutation  $p_M$ , the mutation leads to the time instant equal:

$$\underline{C}_1(1) + x_1$$

where  $x_1$  is a random number that belongs to the interval  $] - \underline{C}_1(1) + \epsilon, \underline{C}_1(2) - \underline{C}_1(1) - \epsilon[$ .

After mutating the first time instant,  $\underline{C}_1$  becomes:

$$\underline{C}_1 = [\tau_1^f + x_1, \tau_2^f, \dots, \tau_{k-1}^f, \tau_k^m, \dots, \tau_N^m] \quad (72)$$

More generally, for  $m \in \llbracket 1, N \rrbracket$ , the mutation leads to the  $m^{th}$  time instant equal to:

$$C_1(m) + x_m \quad (73)$$

where  $x_m \in ]C_1(m-1) - C_1(m) + \epsilon, C_1(m+1) - C_1(m) - \epsilon[$  with  $C_1(0) = 0$ . If  $r > p_M$ , the value of the time instant is not changed.

The selection, crossover, and mutation are repeated until  $N$  new candidates are created. Then, the best  $N$  candidates among the new candidates and those of the  $i^{th}$  population are selected to create the population at the  $(i+1)^{th}$  generation.

### 4.3. Second GA-based approach (NSGA-II)

When solving multi-objective problems, practitioners may be interested in a set of Pareto-optimal solutions<sup>6</sup>. For this purpose, the NSGA was one of the first evolutionary algorithms proposed to find the Pareto-optimal solutions in one single simulation run [36]. However, due to its computational complexity and lack of elitism, Deb *et al.* proposed an improved version called NSGA-II [29] to overcome the aforementioned drawbacks with the advantages of better convergence and higher speed.

As in GA, an initial population is first generated based on the optimization problem. Then, the candidates of the initial population are sorted according to non-domination levels into fronts. Afterward, a crowding distance, which measures how close each candidate is to its neighbors in the same front, is computed for each candidate. As for the selection, the individuals are selected using a tournament selection based on the front rank and the crowding distance. The genetic operators used to produce the offspring population are the simulated binary crossover and the polynomial mutation. Finally, the population that consists of the initial population and the offspring population are sorted according to the front rank. The best

candidates are selected for the next generation. This process is repeated until convergence.

In this paper, when NSGA-II is used with the proposed waveform, with the constraint (58), the simulated binary crossover and the polynomial mutation are replaced by the crossover and the mutation we proposed in the section 4.2.

### 4.4. Conclusions on the two approaches

Two philosophies are hence considered in this paper: On the one hand, the practitioner *a priori* decides the values of the weights  $\lambda_1$  and  $\lambda_2$  in the fitness function. One solution is then obtained by using a GA-based approach. It should be noted that the method could be iterated several times by using different values of the weights in the fitness function. This would lead to a set of solutions that may favor the first, the second, or the third criterion, depending on the values of the weights. In this case, one solution would be associated to a specific set of weights and the number of potential solutions would depend on the number of times the GA algorithm is launched. On the other hand, a Pareto front can be directly obtained by using the NSGA-II algorithm. In this case, the set of solutions is discrete, and its size depends on the parameters of the NSGA-II, such as the population size. In both philosophies, given the specifications in terms of PSLR, ISLR and range resolution, the practitioner can select one solution among all the proposed ones. In the next section, we use both approaches to select the time instants characterizing our transmitted waveform.

## 5. Simulations and results

In this section, the results obtained using GA are presented. This section is organized as follows: firstly, the simulation protocol is given. The results obtained by using the first method combining a single fitness with GA are given. Then, the results obtained with the second method based on NSGA-II are presented. Finally, general comments on the results are provided.

### 5.1. Simulation protocol

In the simulations, we focus on the tangent-based NLFM that has the following parameters:  $T_p = 20 \mu s$ ,  $B = 100$  MHz. The value of  $\beta$  can be selected by the user. In this paper, given the evolutions of PSLR, ISLR,  $R_{res}$  with respect to  $\beta$  in Appendix A, the value of  $\beta$  is chosen equal to 1.22 for two reasons: 1) to approximate a tangent-based NLFM waveform with high degree of non-linearity 2) to have a compromise between  $PSLR_{ref}$  and  $ISLR_{ref}$  on the one hand and  $R_{res,ref}$  on the other hand. In addition, the reference measures that are considered in the optimization issue are given in Table 1.

To illustrate our point, three values of  $N$  are considered, namely  $N = 1, 2$  and  $10$ . This makes it possible to highlight how the performance of the algorithm evolve when

<sup>6</sup>A solution is called Pareto optimal, if there does not exist another solution that dominates it.

Table 1: Reference measures taken into account for the optimization issue based on GA.

$PSLR_{ref}$ (dB)	$ISLR_{ref}$ (dB)	$R_{res,ref}$ (m)
-31.2	-25	1.37

$N$  increases. Concerning GA, the size of the population  $Q_p$  is equal to 200 for  $N = 1, 2$  and 1000 for  $N = 10$ . The probability of mutation  $p_M$  is set at 0.1 and  $\epsilon = 0.12 \mu s$ .

### 5.2. Simulation results of 1<sup>st</sup> method combining a single fitness function and GA

In this section, the parameters and the performance measures obtained for different values of  $N$  are presented. Let us start with the case when  $N = 1$ .

#### 5.2.1. Waveform parameters for $N = 1$

Let us first address the case when the weights are selected as follows:  $\lambda_1 = 0.4$  and  $\lambda_2 = 0.2$ . Given the values of the weights, the PSLR and ISLR has the same level of importance and greater than that of  $R_{res}$ . The time instants as well as the PSLR, the ISLR, and the range resolution that have been obtained using GA are given in Table.2.

Table 2: Performance measures and value of the time instant of the approximated PW-NLFM when  $N = 1$  and GA is used with  $\lambda_1 = 0.4$  and  $\lambda_2 = 0.2$ .

Time instants ( $\mu s$ )	PSLR (dB)	ISLR (dB)	$R_{res}$ (m)
$\tau_1 = 1.6099$	-20.4486	-13.2833	1.1892

In addition, the sampling frequency at the receiver is equal to 100 MHz. Moreover, the time evolution of the instantaneous frequency of the tangent-based waveform, as well as the piecewise-linear approximation optimized by taking into account the criterion (68) are provided in Fig.10.

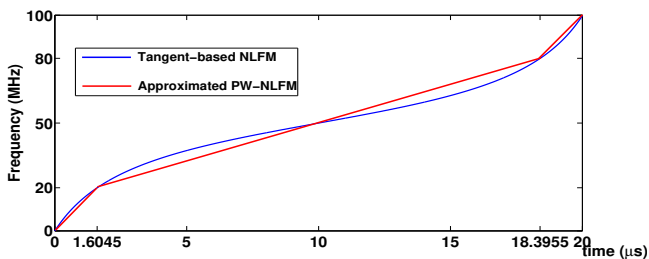


Figure 10: Instantaneous frequency of the tangent-based NLFM waveform and the approximated PW-NLFM waveform when  $N = 1$ ,  $\lambda_1 = 0.4$  and  $\lambda_2 = 0.2$ .  $\tau_1 = 1.6099 \mu s$

Let us now address the case when the weights vary. Thus,  $\lambda_1$  varies between 0.1 and 1, and  $\lambda_2$  varies between 0 and  $1 - \lambda_1$ , both with a step equal to 0.1. In Fig. 11-14, the time instant, the PSLR, the ISLR, and the range resolution are respectively presented as functions of  $\lambda_1$  and  $\lambda_2$ .

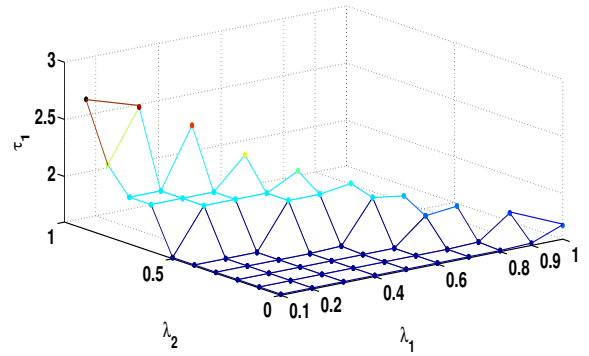


Figure 11: Time instant versus  $\lambda_1$  and  $\lambda_2$  obtained with the 1<sup>st</sup> method when  $N = 1$

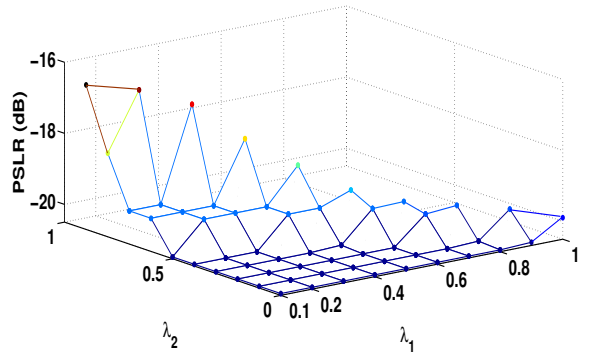


Figure 12: PSLR versus  $\lambda_1$  and  $\lambda_2$  obtained with the 1<sup>st</sup> method when  $N = 1$

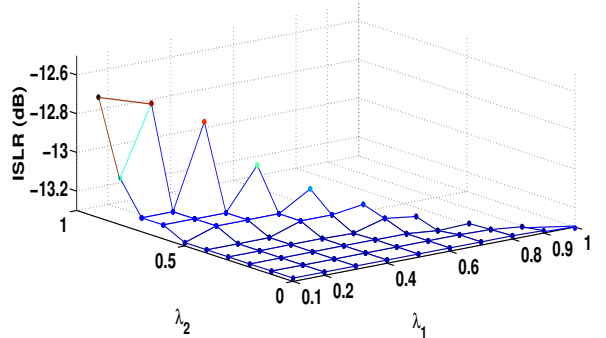


Figure 13: Value of the ISLR versus  $\lambda_1$  and  $\lambda_2$  obtained with the 1<sup>st</sup> method when  $N = 1$

Let us look at  $\lambda_1 = 0.1$ . In this case, based on (68), the performance in terms of ISLR does not necessarily play a key role in the criterion. For values of  $\lambda_2$  smaller than 0.4, the time instant  $\tau_1$  does not change. In addition, the range resolution is the same and smaller than  $R_{res,ref}$ . When  $\lambda_2$  increases, the time instant and the range resolution increase. The latter becomes closer and closer to

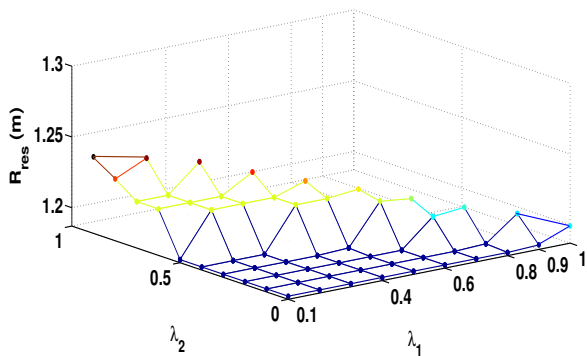


Figure 14: Range resolution versus  $\lambda_1$  and  $\lambda_2$  obtained with the 1<sup>st</sup> method when  $N = 1$

$R_{res,ref}$ .

Given Fig. 12, we can observe that for small values of  $\lambda_1$  and  $\lambda_2$ , the PSLR is the closest one to  $PSLR_{ref}$ . Indeed, in these cases, the criterion  $F(\underline{x})$  is mainly defined by the normalized difference on the PSLR. When the sum of  $\lambda_1$  and  $\lambda_2$  becomes closer to 1,  $F(\underline{x})$  is mainly defined by the normalized differences on the ISLR and the range resolution; one can notice that the PSLR increases. For instance, for  $\lambda_1 = 0.1$  and  $\lambda_2 < 0.6$ , the PSLR remains unchanged. When  $\lambda_1$  increases, the PSLR increases. The performance measures presented in Fig. 11-14 make it possible to define a set of solutions for the multi-objective optimization issue which are each associated to a set of weights. Moreover, based on the time instants presented in Fig.11, the sampling frequency at the receiver is equal to 100 MHz for any set of weights.

In Fig. 15, the performance measures obtained for different set of weights are presented. When comparing the values of the PSLR, the ISLR, and the range resolution we obtain with the performance measures of reference, the difference can be significant (*e.g.* at least 10 dB for the PSLR). This is probably due to the strong approximation that is made when only one time instant is used. Thus, increasing  $N$  should reduce it. For this reason, in the next section,  $N = 2$  is considered.

### 5.2.2. Waveform parameters, for $N = 2$

The weights are still selected as follows:  $\lambda_1 = 0.4$  and  $\lambda_2 = 0.2$ . The results are presented in Table. 3 and Fig.16. We can notice that increasing  $N$  to 2 reduces the normalized differences on the performance measures.

Table 3: Performance measures and the values of the time instants of the approximated PW-NLFM when  $N = 2$ .

Time instants ( $\mu s$ )	PSLR (dB)	ISLR (dB)	$R_{res}$ (m)
$\tau_1=2.2970$ ; $\tau_2=5.0211$	-24.7427	-16.0011	1.3107

Let us now see how the waveform parameters evolve when the weights change. To this end,  $\lambda_1$  varies between 0.1 and

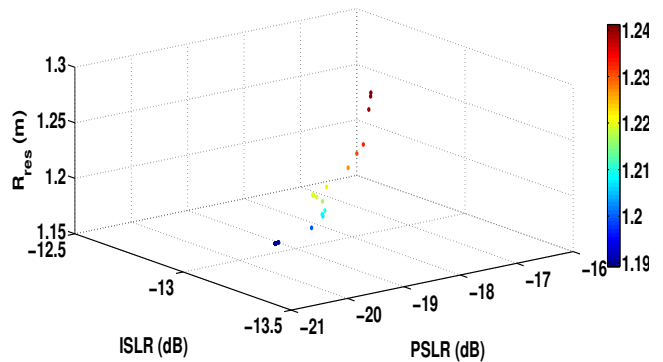


Figure 15: Performance measures obtained with the 1<sup>st</sup> method using different weights when  $N = 1$ .

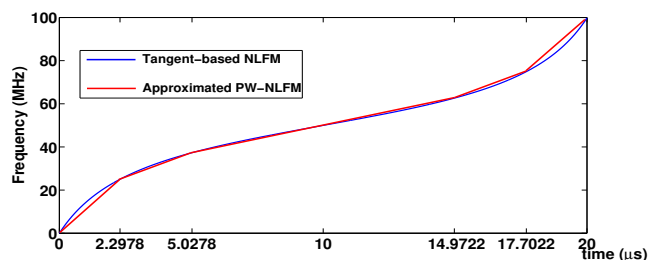


Figure 16: Instantaneous frequency of the tangent-based NLFM waveform and the approximated PW-NLFM waveform when  $N = 2$ .

1, and  $\lambda_2$  still varies between 0 and  $1 - \lambda_1$ , both with a step equal to 0.1. In Fig. 17-20, the PSLR, ISLR, the range resolution, and the sampling frequency at the receiver are respectively presented as functions of  $\lambda_1$  and  $\lambda_2$  when  $N = 2$ .

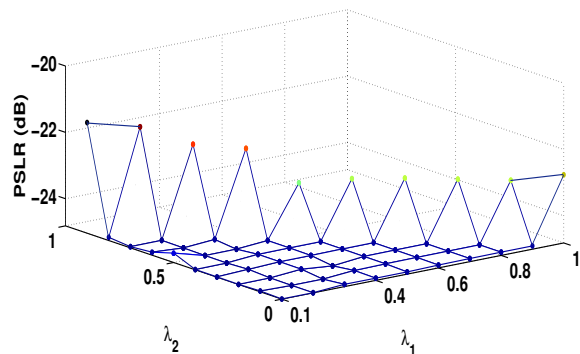


Figure 17: PSLR versus  $\lambda_1$  and  $\lambda_2$  obtained with the 1<sup>st</sup> method when  $N = 2$ .

For a fixed value of  $\lambda_1$ , when  $\lambda_1 + \lambda_2 = 1$ , the PSLR takes the maximum value. This is coherent with the fact that the criterion to be optimized no longer depends on the PSLR. When  $\lambda_1 = 0.1$  and  $\lambda_2 = 0$ , the PSLR is the closest one to  $PSLR_{ref}$ . In this case, a great importance is given to the PSLR. Let us now look at  $\lambda_1 = 0.3$ . For values of  $\lambda_2$  smaller than 0.7, the PSLR is almost the same.

Given Fig. 18, the ISLR takes the maximum value when

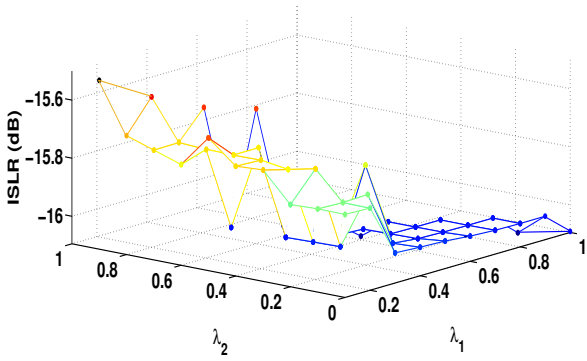


Figure 18: ISLR versus  $\lambda_1$  and  $\lambda_2$  obtained with the 1<sup>st</sup> method when  $N = 2$

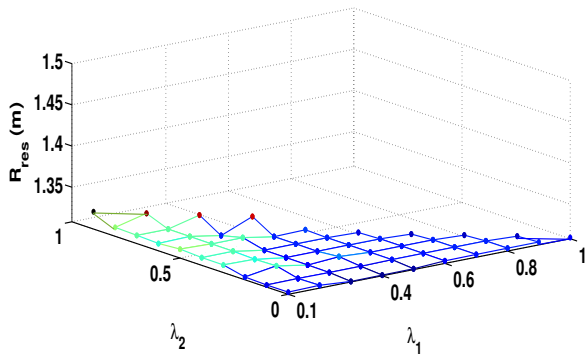


Figure 19: Range resolution versus  $\lambda_1$  and  $\lambda_2$  obtained with the 1<sup>st</sup> method when  $N = 2$

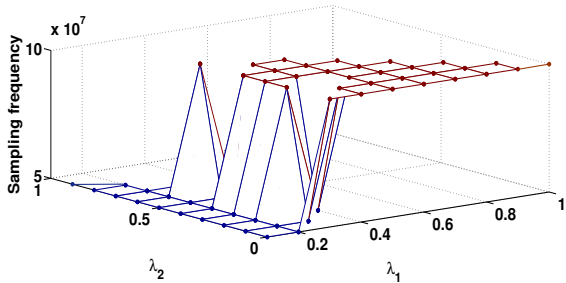


Figure 20: Sampling frequency versus  $\lambda_1$  and  $\lambda_2$  obtained with the 1<sup>st</sup> method when  $N = 2$

$\lambda_1 = 0.1$  and  $\lambda_2 = 0.9$  and the minimum value when  $\lambda_1 = 1$  and  $\lambda_2 = 0$ .

According to Fig. 20, the sampling frequency at the receiver depends on  $\lambda_1$  and  $\lambda_2$ . It takes two distinct values: 50 MHz and 100 MHz.

In Fig. 21, the performance measures obtained for different set of weights are presented. As a conclusion, when  $N$  is equal to 2, the performance measures become closer to the reference ones. Moreover, the sampling frequency at the receiver could be reduced.

We may *a priori* imagine that increasing the number of instants more and more should lead to better performance

measures and a smaller sampling frequency at the receiver. For this reason, in the following section and after various simulation tests we did, we suggest optimizing the waveform parameters when  $N = 10$ .

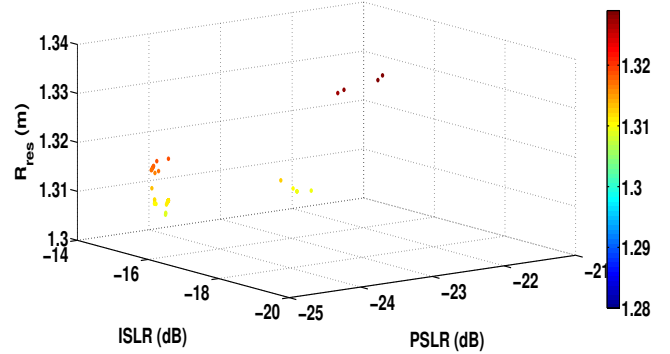


Figure 21: Performance measures obtained with the 1<sup>st</sup> method using different weights when  $N = 2$ .

### 5.2.3. Waveform parameters, for $N = 10$

In this section, the waveform parameters when  $N = 10$  are optimized by using GA for  $\lambda_1 = 0.4$  and  $\lambda_2 = 0.2$ . In this case,  $Q_p$  is equal to 1000. The results are presented in Table. 4. Based on the time instants provided in Table. 4, the sampling frequency that should be used is equal to 33.3333 MHz.

Given Table. 4, we can observe that the normalized differences on the PSLR and the range resolution are approximately equal to zero. As for normalized difference on the ISLR, it is equal to 0.1171. It is worth-noting that the value of  $N$  has been arbitrarily chosen to be relatively large to show the potential of our arrangement in order to be as close as possible to one or more of the reference performance measures.

Table 4: Performance measures and the values of the time instants of the approximated PW-NLFM when  $N = 10$ .

Time instants ( $\mu s$ )	PSLR(dB)	ISLR(dB)	$R_{res}$ (m)
$\tau_1=0.7658; \tau_2=2.2058$	-31.2	-22.0713	1.3816
$\tau_3=3.2628; \tau_4=4.2901$			
$\tau_5=5.4037; \tau_6=6.2491$			
$\tau_7=7.2719; \tau_8=8.7119$			
$\tau_9=9.3766; \tau_{10}=9.5402$			

### 5.2.4. Conclusions concerning the 1<sup>st</sup> method combining a single fitness function and GA

We have analyzed three different cases:  $N = 1$ ,  $N = 2$  and  $N = 10$ . As expected, the larger  $N$ , the better the performance and the smaller the sampling frequency. Moreover, the time it takes to send all the pulses is large. In each case, depending on the weights *a priori* chosen by the practitioner, one solution can be obtained. In the following section, we search for a set of non-dominated solutions

by minimizing the normalized errors on the performance measures using NSGA-II.

### 5.3. Simulation results of the 2<sup>nd</sup> method based on NSGA-II

In this section, we aim at finding the Pareto-optimal solutions using NSGA-II. The objective functions to be minimized are the normalized errors on the PSLR, ISLR, and  $R_{res}$  *i.e.* (65), (66) and (67). In Fig. 22 and Fig. 23, the Pareto fronts obtained when  $N = 1$  and 2 are respectively presented. It is up to the practitioner to choose one of the non-dominated solutions depending on the performance measures needed in his application.

Moreover, we noticed that all the solutions obtained with GA for different set of weights in Fig. 15 and Fig. 21 exist in the Pareto front obtained with NSGA-II with a very slight difference.

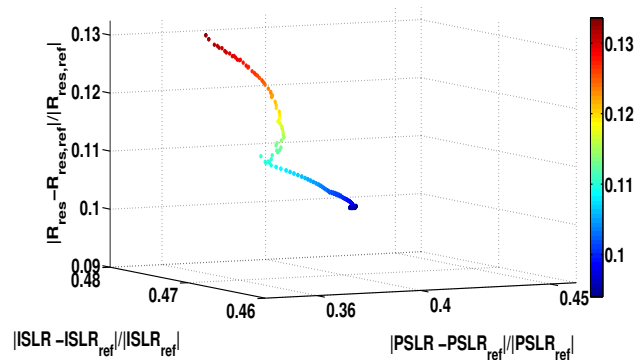


Figure 22: Pareto front obtained with the 2<sup>nd</sup> method based on NSGA-II when  $N = 1$

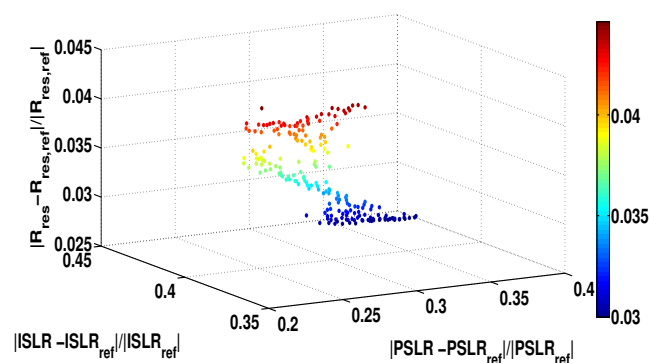


Figure 23: Pareto front obtained with the 2<sup>nd</sup> method based on NSGA-II when  $N = 2$

### 5.4. General comments on the results

We have presented the results obtained using two methods. The second method requires a computational cost

smaller than that of the first method when the latter is iterated. Moreover, we noticed that increasing the number of time instants *i.e.*, the number of pulses within the CPI, leads to performances closer to the reference ones and reduces the sampling frequency at the receiver.

In practice, the CPI is limited by several factors. These factors depend on the application of the radar. For instance, in radar target classification, the CPI is limited by the speed of the target. In scenarios where the speed of the target is fast, the dwell time<sup>7</sup> is small. Thus only a small number of time instants can be used. On the contrary, in scenarios where the speed of the target is small or moderate, a larger number of time instants could be used. Therefore, a trade-off exists between the number of time instants, on the one hand, the performance measures and the sampling frequency, on the other hand.

## 6. Analyzing the relevance of our approach in alternative scenarios

In this section, we aim at analyzing the relevance of our approach in alternative scenarios such as multiple scatterers and Doppler effect. It should be noted that these assumptions were not taken into account in the mathematical development presented in section 3. The general parameters used are:  $T_p = 20 \mu s$ ,  $T_r = 10000$ ,  $f_c = 3$  GHz, and  $N = 10$ . The time instants used to generate the waveform are those provided in Table. 4. Let us start with the scenario when echoes from multiple scatterers are received at the receiver.

### 6.1. HRRP of a stationary target

In this subsection, the HRRP of a stationary point target obtained using the TD algorithm is compared with that obtained using the MF. The target is located at range  $R = 1440$  m. In Fig. 24, the HRRPs obtained by using both algorithms are presented. The PSLR and the ISLR obtained using the TD algorithm are much better than those obtained using the MF. This is due to the fact that by using the MF, the train of variable chirp pulses are not processed in the appropriate way that permits the reconstruction of the PW-NLFM waveform at the receiver. This sheds light on the indispensable role of the processing steps namely, interpolation, frequency shift, time shift, and phase correction, that should precede the MF, as illustrated in section 3.3.

In order to see the influence of the performance measures on detection, let us suppose it is required to detect and identify a certain target from some of its scatterers. In this case, let us assume three point scatterers with reflection coefficients  $[\alpha_1 A_1, \alpha_2 A_2, \alpha_3 A_3] = [1, 0.8, 0.1]$ . The ranges

<sup>7</sup>It is the time that an antenna beam spends on a target. It can correspond to the duration of one CPI or more CPIs.

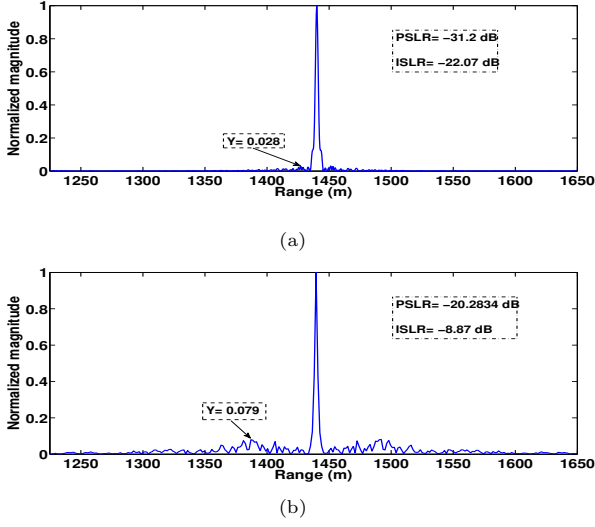


Figure 24: HRRP of a stationary point target obtained using (a) TD algorithm (b) matched filter.

between the scatterers and the radar are  $[R_1, R_2, R_3] = [1420\text{ m}, 1440\text{ m}, 1470\text{ m}]$ , as shown in Fig. 25. It is obvious that the third scatterer with the lowest RCS cannot be distinguished from the sidelobes of the other two scatterers with larger RCSs when the proposed waveform is processed with MF.

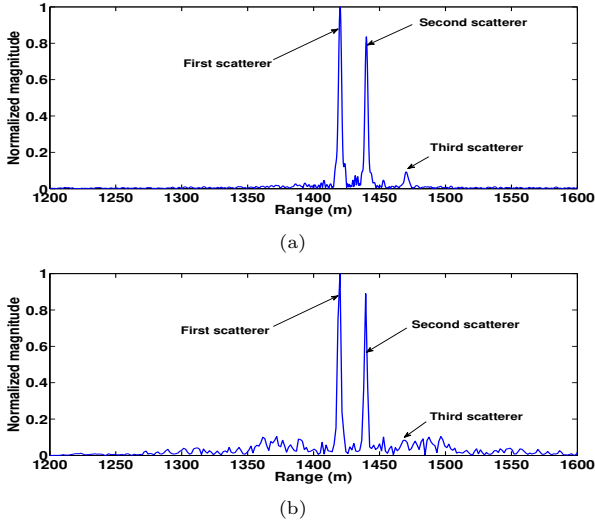


Figure 25: HRRP of a stationary point target that consists of three scatterers obtained using (a) TD algorithm (b) matched filter.

### 6.1.1. Influence of Doppler on the HRRP

In this subsection, we aim at analyzing the influence of Doppler on the HRRP of the VCR SF-LFM waveform. For this purpose, three scenarios with different target velocities are considered. In this simulation, the target is located at range  $R = 1440\text{ m}$ .

In figures 26, 27, and 28, the HRRP of the VCR SF-LFM waveform obtained for relatively low, moderate, and high speeds namely,  $v=50\text{ m/s}$ ,  $150\text{ m/s}$ , and  $250\text{ m/s}$  are

respectively presented. The received echoes are processed using both the generalized version of the TD algorithm, and the MF algorithm. It is worthy to note that by applying the MF directly to the received echoes, the reconstructed waveform is no longer a PW-NLFM waveform but rather an ordinary SF-LFM waveform. Whatever the speed of the target, the attenuation that results from the Doppler shift is relatively less severe in case of the TD algorithm than the MF algorithm. As for the range shift, at low and moderate speeds, the MF slightly outperforms the TD. However, at high speeds the range shifts are similar.

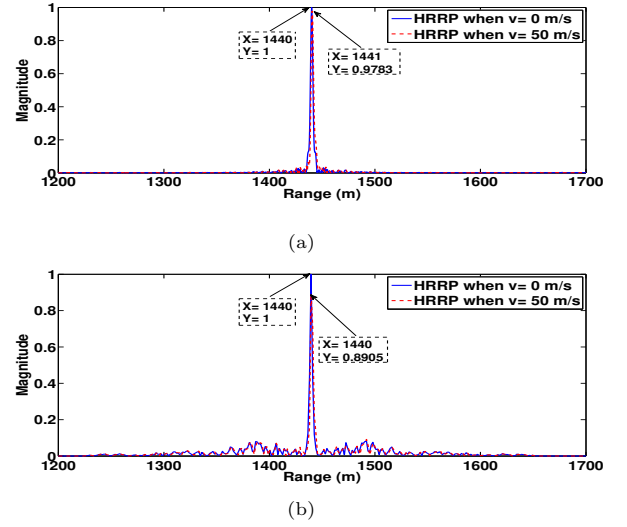


Figure 26: HRRP of a moving target with  $v=50\text{ m/s}$  obtained using (a) TD algorithm (b) matched filter.

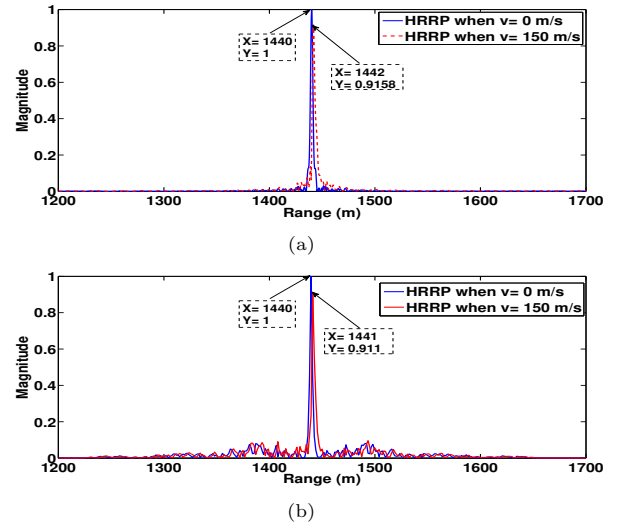


Figure 27: HRRP of a moving target with  $v=150\text{ m/s}$  obtained using (a) TD algorithm (b) matched filter.

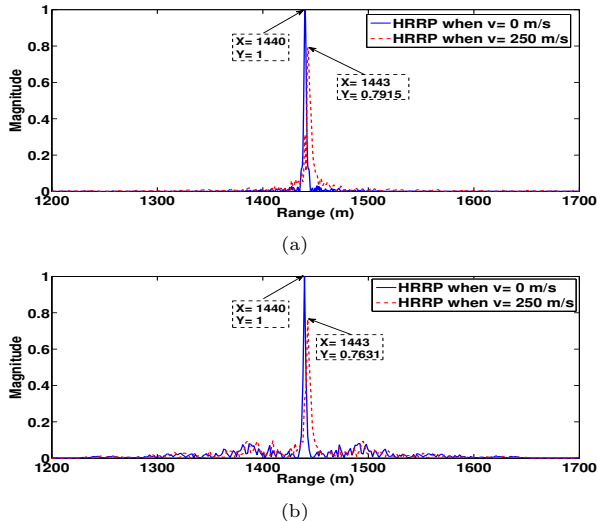


Figure 28: HRRP of a moving target with  $v=250 \text{ ms}^{-1}$  obtained using (a) TD algorithm (b) matched filter.

## 7. Conclusions and perspectives

Two evolutionary methods have been evaluated to estimate the parameters of the variable-chirp rate SF-LFM waveform, whose processing chain from the transmitter to the receiver has been described in the paper. If the practitioner wants to analyze different cases, the first approach based on GA can be iterated for different set of weights, whereas the second approach based on NSGA-II directly provides a Pareto front. According to the simulations we conducted for one scatterer, the NSGA-II-based method is probably the more suitable due to its smaller computational cost. The approach has been also tested in scenarios with multiple scatterers or Doppler effect. The results are promising. In the future, we aim at designing the same type of approach without referring to a tangent-based NLFM method. In this case, the time instants as well the frequency band will have to be estimated to tend to PSLR, ISLR, and range resolution the practitioner will *a priori* define.

## 8. Acknowledgements

This project has been funded with support from the National Council for Scientific Research in Lebanon.

### Appendix A: PSLR, ISLR, and $R_{res}$ of tangent-based NLFM waveform

The PSLR, ISLR, and  $R_{res}$  of a tangent-based NLFM waveform vary when  $\beta$  varies. In Fig. 29, the PSLR and the ISLR are presented for different values of  $\beta$ . When  $\beta \in [0, 0.9]$ , the instantaneous frequency given in Fig 1 is close to a linear function of the time. The resulting PSLR

and the ISLR tend to evolve in a smooth way. When  $\beta$  becomes larger, the degree of non-linearity is more significant. In this case, the performance in terms of PSLR and ISLR vary much. In Fig. 30, the range resolution versus  $\beta$  is presented. As  $\beta$  increases, the range resolution increases.

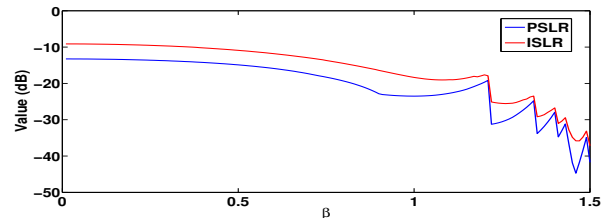


Figure 29: PSLR and ISLR versus  $\beta$  when  $B = 100 \text{ MHz}$ .

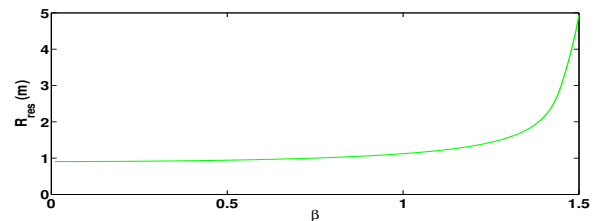


Figure 30: Range resolution versus  $\beta$  when  $B = 100 \text{ MHz}$ .

## References

- [1] M. A. Richards, J. A. Scheer, W. A. Holm, Principles of modern radar, Vol. I: Advanced techniques, SciTech Publishing, 2010.
- [2] Z. Ge, P. Huang, W. Lu, Matched NLFM pulse compression method with ultra-low sidelobes, In Proceedings of the 5th European Radar Conference (2008) 92–95.
- [3] M. Skolnik, Radar handbook, McGraw-Hill Book Co., United states, 2008.
- [4] T. Collins, Active sonar pulse designs, PhD, University of Birmingham, 1996.
- [5] W. L. Melvin, J. A. Scheer, Principles of modern radar, Vol. II: Advanced techniques, SciTech Publishing, 2013.
- [6] S. Boukeffa, Y. Jiang, T. Jiang, Sidelobe reduction with nonlinear frequency modulated waveforms, 2011 IEEE 7th International Colloquium on Signal Processing and its Applications (2011).
- [7] C. Pang, P. Hoogeboom, F. Chevalier, H. W. Russchenberg, J. Dong, T. Wang, X. Wang, A pulse compression waveform for weather radars with solid-state transmitters, IEEE Geoscience and Remote Sensing Letters 12 (2) (2015) 2026–2030.
- [8] G. Jin, K. Liu, Y. Deng, Y. Sha, R. Wang, D. Liu, W. Wang, Y. Long, Y. Zhang, Nonlinear frequency modulation signal generator in lt-1, IEEE Geoscience and Remote Sensing Letters 16 (10) (2019) 1570 – 1574.
- [9] E. D. Witte, H. D. Griffiths, Improved ultra-low range sidelobe pulse compression waveform design, Electronic Letters 40 (22) (October 2004).
- [10] J. Saeedi, K. Faez, Synthetic aperture radar imaging using nonlinear frequency modulation signal, IEEE Transactions on Aerospace and Electronic Systems 52 (1) (2016) 99–110.
- [11] R. T. Lord, Aspects of stepped-frequency processing for low-frequency SAR systems, PhD thesis, University of Cape Town, Dept of Electrical Engineering, 2000.
- [12] D. R. Wehner, High resolution radar, Artech House, London, UK, 1995.

- [13] A. J. Wilkinson, R. T. Lord, M. R. Inggs, Stepped-frequency processing by reconstruction of target reflectivity spectrum, *Proceedings of the South African Symposium on Communications and Signal Processing* (September 1998).
- [14] D. A. Ausherman, A. Kozma, J. L. Walker, H. M. Jones, E. C. Poggio, Developments in radar imaging, *IEEE Transactions on Aerospace and Electronic Systems* 20 (4) (1984) 363–400.
- [15] M. Y. Chua, V. C. Koo, H. S. Lim, J. . T. S. Somantyo, Phase coded stepped frequency linear frequency modulated waveform synthesis technique for low altitude ultra wideband synthetic aperture radar, *IEEE Access* 5 (2017) 11391–11403.
- [16] R. Liu, Y. Wang, Imaging approach for airborne stepped-frequency synthetic aperture radar in the squinted mode, *Journal of applied remote sensing* 11 (1) (2017) 1–15.
- [17] X. Luo, Y. Deng, R. Wang, W. Xu, L. Guo, Imaging for MIMO sliding spotlight SAR using stepped frequency chirps, *EUSAR, 10th European Conference on Synthetic Aperture Radar* (2014).
- [18] Q. Zhang, Y. Q. Jin, Aspects of radar imaging using frequency-stepped chirp signals, *EURASIP Journal on Applied Signal Processing* (2006) 1 – 8.
- [19] C. Fukushima, N. Hamada, A study on stepped frequency radar by using intra-pulse phase coded modulation, *Proceedings of the World Congress on Engineering and Computer Science* (October 2008).
- [20] T. Li, H. Yang, , Z. Zhou, RFI suppression based on phase-coded stepped-frequency waveform in through-wall radars, *IEEE Transactions on Geoscience and Remote Sensing* 53 (2015) 1583–1591.
- [21] I. Gladkova, D. Chebanov, Grating lobes suppression in stepped-frequency pulse train, *IEEE Transactions on Aerospace and Electronic Systems* 44 (2008) 1265 – 1275.
- [22] I. Gladkova, Analysis of stepped-frequency pulse train design, *IEEE Transactions on Aerospace and Electronic Systems* 45 (5) (2009) 1251 – 1261.
- [23] V. Kumar, A. K. Sahoo, Grating lobe and sidelobe suppression using multi-objective optimization techniques, in: *IEEE ICCSP 2015 conference*, 2015, pp. 247–251.
- [24] F. Zhu, Q. Zhang, Q. Lei, Y. Luo, Reconstruction of moving target’s hrrp using sparse frequency-stepped chirp signal, *IEEE sensors journal* 11 (10) (2011) 2327 – 2334.
- [25] M. Saleh, S.-M.Omar, E. Grivel, O. Bazzi, A modified stepped frequency phase coding radar waveform designed for the frequency domain algorithm, *Digital Signal Processing* (88) (2019) 101–115.
- [26] M. Saleh, S.-M. Omar, E. Grivel, Diversifying the processing chain of the modified stepped frequency radar waveform combined with pulse compression techniques, *IEEE Radar Conference (RADAR)* (2020).
- [27] G. Galati, G. Pavan, Waveforms design for modern and mimo radar, *IEEE EUROCON* (2013).
- [28] X. Xu, R. M. Narayanan, Range sidelobe suppression technique for coherent ultra wide-band random noise radar imaging, *IEEE Transactions on Antennas and Propagation* 49 (12) (2002) 1836–1842.
- [29] K. Deb, A. Pratap, S. Agarwal, T. Meyarivan, A fast and elitist multiobjective genetic algorithm: Nsga-ii, *IEEE Transactions on Evolutionary computation* 6 (2) (2002) 182–197.
- [30] D. R. Wehner, *High resolution radar*, Artech House, London, UK, 1995.
- [31] H. Meikle, *Modern Radar Systems*, Artech House, 2008.
- [32] W. E. Alexandar, C. M. Williams, *Digital Signal Processing: Principles, Algorithms and System Design*, John Wiley & Sons, Inc., Hoboken, New Jersey, NC, USA, 2016.
- [33] D. E. Goldberg, *Genetic Algorithms in Search, Optimization and Machine Learning*, Addison-Wesley Longman, Boston, MA, USA, 1989.
- [34] C. S. Chin, W. P. Lin, Robust genetic algorithm and fuzzy inference mechanism embedded in a sliding-mode controller for an uncertain underwater robot, *IEEE/ASME Transactions on Mechatronics* 23 (2) (2018) 655 – 666.
- [35] A. Saldivar, C. Goh, Y. Li, Y. Chin, H. Yu, Identifying smart design attributes for industry 4.0 customization using a clustering genetic algorithm, *22nd International Conference on Automation and Computing (ICAC)* (October 2016).
- [36] N. Srinivas, K. Deb, Multiobjective optimization using non-dominated sorting in genetic algorithms, *Evolutionary Computation* 2 (3) (1994) 221–248.